AFATL-TR-68-43

2.75-Inch FFAR Large Yaw Dynamics

by

Carroll B. Butler

AFATL TECHNICAL REPORT AFATL-TR-68-43

MARCH 1968

AIR FORCE ARMAMENT LABORATORY
AIR FORCE SYSTEMS COMMAND
EGLIN AIR FORCE BASE, FLORIDA

2.75-INCH FFAR LARGE YAW DYNAMICS

by

Carroll B. Butler

FOREWORD

This report presents basic data and analysis techniques for obtaining $C_{m_q} + C_{m_{\dot{\alpha}}}$ and C_{m_α} from a single degree of freedom using the method of differential corrections to fit the motion to the linear theory. The report was originally submitted to the University of Notre Dame Graduate School as a thesis topic.

This report has been reviewed and is approved.

for JOSEPH E. DUVAL, Colonel, USAF
Chief, Ballistics Division

ABSTRACT

Dynamic tests were conducted in the 24-inch Subsonic Wind Tunnel at the Notre Dame Aero-Space Department to investigate primarily the large yaw dynamic characteristics of the 2.75-inch FFAR, utilizing a unique model support system which provides single degree of freedom motion. From the free pitching motion the stability coefficients C_{m_α} and C_{m_q} were obtained for the 2.75-inch FFAR at low subsonic Mach numbers, and at angles of attack up to 60 degrees by fitting the motion to the Linear Theory utilizing the Method of Differential Corrections. Nonlinear effects due to variations in free oscillation frequency are considered. Static test results are also included from tests conducted at the Arnold Engineering Development Center. These latter tests were conducted over a Mach number regime of $M_\infty = .6 \rightarrow 5.0$ and angle of attack range of $\alpha = -4 \rightarrow 12$ degrees.

(The reverse of this page is blank.)

CONTENTS

ILLUSTRATIONS AND TABLES

(The reverse of this page is blank.)

DEFINITION OF SYMBOLS

C_A	Axial force coefficient.
CP	Center of pressure.
C_m	static pitching moment coefficient.
C_{m_q}	pitch damping moment coefficient defined as for consistency with "Wobble" output.
$C_{m_{\dot{\alpha}}}$	pitching moment coefficient due to lag ($\dot{\alpha}$).
$C_{m_{\delta_e}}$	pitching moment due to control surface deflection.
$C_{Z_\alpha}, C_{N_\alpha}$	normal force coefficient.
$C_{Z_\alpha}, C_{N_\alpha}$	normal force slope coefficient.
$C_{Z_{\dot{\alpha}}}$	normal force slope due to lag ($\dot{\alpha}$).
C_{Z_q}	pitch damping normal force coefficient.
$C_{Z_{\delta_e}}$	normal force slope coefficient due to control surface deflection.
d	reference length, body diameter.
i	$\sqrt{-1}$.
I	transverse moment of inertia.
M_∞	free stream mach number.
M_α	static pitching moment slope.
M_q	pitch damping moment slope due to q.
$M_{\dot{\alpha}}$	moment slope due to lag ($\dot{\alpha}$).
M_{δ_e}	moment slope due to control surface deflection.

N_1, N_2, N_3	Coefficients used in equation (2).
q	pitching velocity.
Q	dynamic pressure.
R	Reynolds number.
S	reference area.
V	velocity.
Z_α	normal force slope.
Z_q	damping force slope due to q.
$Z_{\dot{\alpha}}$	normal force slope due to lag ($\dot{\alpha}$).
Z_{δ_ϵ}	normal force slope due to control surface deflection.
α	angle of attack.
$\dot{\alpha}_o, \alpha_o$	angle of pitch and rate of change of angle of attack at time zero.
α_T	trim angle of attack.
δ	phase angle between peak amplitude and time zero.
δ_ϵ	control surface deflection.
φ	$\lambda + i\omega$.
ρ	density.
λ	damping factor.
λ_o	damping factor at time zero.
θ	pitch attitude.
ω	frequency.

INTRODUCTION

An investigation of the dynamic stability characteristics of the 2.75-inch FFAR is accomplished from wind tunnel test results utilizing the Linear and Nonlinear Theory of Nicolaides, Ref. 1, and applies current state of the art data reduction and testing techniques developed by the Notre Dame Aero-Space Department.

The classical linear solution is summarized for the single degree of freedom case and shown to be

$$\alpha = \alpha_T + K e^{\lambda t} \cos(\omega t + \delta)$$

The nonlinear case is then developed resulting in corrections to the above expression to account for C_{m_α} or ω not remaining constant with changing amplitude. The nonlinear model yields

$$\alpha = \alpha_T + K \sqrt{\frac{\omega_0}{\omega}} \cos(\alpha + \delta) \text{ where } \theta = \int_0^t \omega dt$$

The "wobble" computer program is discussed in some detail. This program was developed by Eikenberry, Ref. 2, and basically utilizes the theory of Nicolaides. Also included are recent techniques developed by NASA in obtaining C_{m_α} and C_{m_q} as functions of angle of attack where the coefficients are nonlinear with angle of attack, Ref. 3 and 4. All data reduction was accomplished utilizing this program. Data are given showing typical outputs from the "Wobble" computer program, and also repetitive data to indicate data consistencies. Computed polynomial expressions for static pitching moment C_{m_α} and pitch damping coefficients C_{m_q} were obtained for the 2.75-inch FFAR at low subsonic Mach numbers at angles of attack from 0 degree → 60 degrees. The dynamic stability tests were conducted in the test facilities at the University of Notre Dame Aero-Space Department.

A unique model support system utilizing synthetic jewels to minimize friction effects was used in the free oscillation tests. Testing techniques developed by Nelson, Ref. 5, under a previous Air Force contract were utilized in the free oscillation single-degree of freedom wind tunnel tests.

This investigation was prompted as a result of a continuous effort to utilize existing hardware for new applications. The 2.75-inch FFAR was originally designed as an air-to-ground weapon and was intended only for forward-firing applications. Numerous modifications in motors and warheads have been accomplished over the years. The XM 151 warhead is currently seeing wide use by the Army, Navy, and Air Force since this particular warhead was designed to provide a rapid fuze reaction time. The weapon has proven to be very effective for forward-firing application. One such installation is shown in Figure 1.

The targets may be specific targets or in many cases the target area may be large. In these cases the question has been raised as to the feasibility of launching the 2.75-inch FFAR sideways from low subsonic aircraft.

One immediate question which one may anticipate is the static and dynamic stability characteristics of the rocket at large angles of attack. This arises since the rocket exit velocity for practical rocket tube lengths would not be expected to exceed 150 feet per second and combining this with a low airspeed-type aircraft, angles of attack of 50 degrees and greater are possible as the rocket exits the tube. A literature search provided practically no information. Dr. Haseltine of the China Lake Test Facility located some NOTS departmental correspondence concerning large yaw side-firing tests of a rocket configuration similar to the 2.75-inch FFAR. These test results were anything but encouraging as rocket instabilities were observed at large angles of attack.

In addition to the current wind tunnel test, the writer has initiated a series of tests at the Holloman AFB sled track facility. These tests are currently underway, Ref. 6. The FFAR results to date have been very encouraging and tend to substantiate the wind tunnel tests insofar as no apparent static or dynamic stability problems have been observed at large angles of attack.

Static wind tunnel data were obtained by the writer at the Arnold Engineering Test Facilities for an angle of attack range of $\alpha = 4$ degrees $\rightarrow$ 12 degrees. No dynamic wind tunnel test data of the 2.75-inch FFAR were previously available at small or large angles of attack, primarily since it is very difficult using conventional sting support systems to handle configurations by the forced oscillation technique which have large fineness ratios. Thus, in addition to obtaining the dynamic

characteristics of the 2.75-inch FFAR, a unique support system was utilized to provide more realistic dynamic data by minimizing friction effects in the support system.

Figure 1. XM 151 Weapon Installation.

THE WIND TUNNEL AND INSTRUMENTATION

The Notre Dame wind tunnel is shown in Figure 2, and the specific instrumentation and model installation are shown in Figure 3. One particularly unique characteristic of this tunnel facility is the very low turbulence levels. This low turbulence level is possible due to an inlet contraction ratio of 20.6/1 and 12 fine mesh screens. The wind tunnel is the open circuit type with continuous flow. Power is provided by a 15-horse-power motor and eight-blade fan assembly with operating Mach numbers in the low subsonic regime (100 feet per second maximum). Fan speed is controlled by a small 24-volt DC motor.

Also shown in Figure 3 is the strobe (strobotac, type 1531-A) camera, and motorized cart used to record the motion. The strobe provides 10 pulses per second and was used to illuminate a small ball bearing located at the apex of the model forebody. The spherical surface provides optimum light reflection characteristics allowing larger camera f/stop setting and larger depths of field.

A 4 x 5 Kodak Master view camera with a Kodak commercial f/6.3, 8.5-inch lens and a number 3 Acme Synchro Shutter was used with Polar Pan type 52 film (ASA = 400) to obtain optimum lighting and f/stop setting. Royal pan film with identical film speed was then used for recording data. Two plate glass sections are used in the bottom of the test section to provide the model image projection.

The camera was mounted on a motorized cart which moves parallel to the last section. The speed of the cart may be varied to provide a maximum number of test points in the exposure.

A Hewlett-Packard electronic counter model 522B, was used to allow vernier adjustments of the strobe to insure exactly 10 pulses per second.

The digital comparator shown in Figure 4 was used to record the model angular position as a function of time, in the form of five-digit numbers in .01 millimeter units.

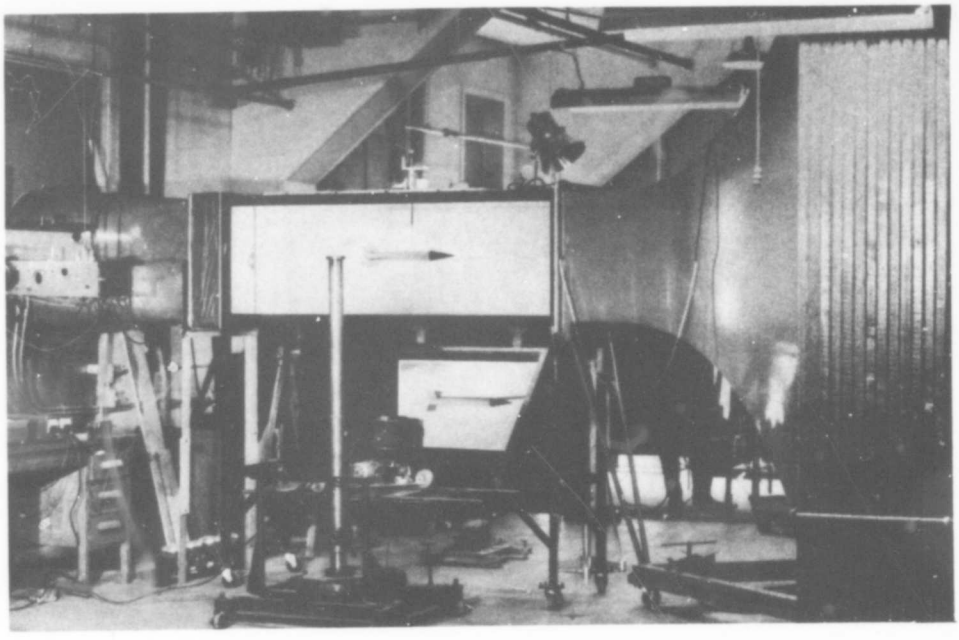

Figure 2. Laboratory Setup.

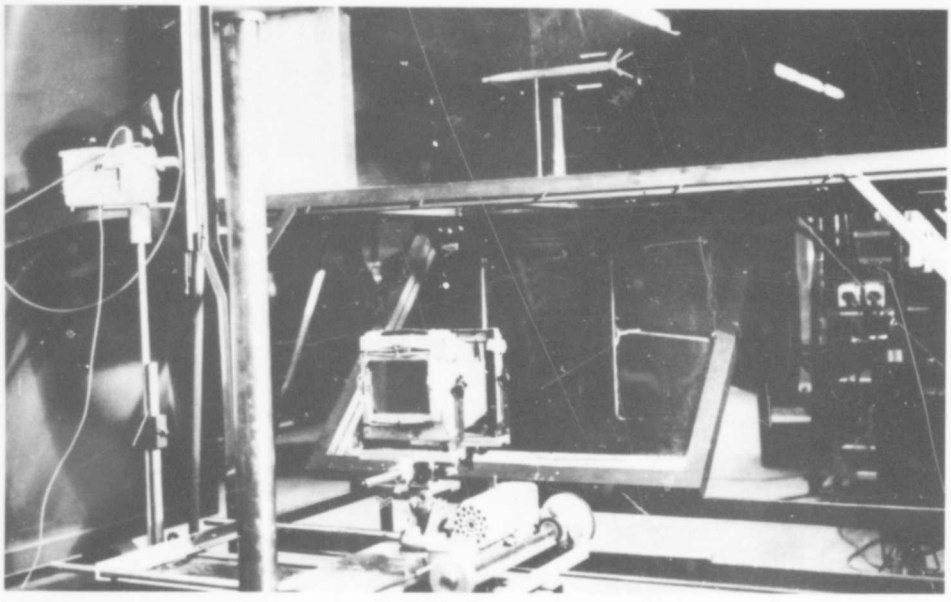

Figure 3. Model Installation and Instrumentation.

Figure 4. Digital Optical Comparator.

MODEL SUPPORT SYSTEM AND MODEL CONFIGURATIONS

The disassembled model support system shown in Figure 5 provides minimal friction effects for free oscillation-type tests. The roller bearing shown near the top of the strut essentially prevents model translatory motion. All model weight is supported by a small cup-shaped glass bearing mounted in the upper end of the small cylinder shown in the lower position of Figure 5.

The bearings used for this test were fabricated in the Notre Dame Aero-Space shop facility. Bearings are also available from the Bulova Watch Company which are made of synthetic sapphire. These bearings have excellent wear resistance due to the material density and hardness. Limited tests were conducted utilizing the cup, vee, and hole jewel. Model configurations utilized in the Notre Dame and AEDC test facilities are shown in Figures 6 and 7.

DETERMINATION OF MOMENT OF INERTIA

The torsional pendulum was utilized to determine the model moment of inertia. In using this technique, the model was supported at the model pivot point by a 5-inch-long .037-inch-diameter wire. The model was given an angular displacement and released and periods were then averaged over a 10-cycle oscillation. Periods were also measured for cylindrical tubing with known moments of inertia which were slightly greater and less than the 2.75-inch FFAR model. A linear plot of oscillation period versus $\sqrt{I}$ is shown in Figure 8. This plot was constructed from the two known end points determined for the cylindrical tubing. The plot was then entered with the measured model period to determine the model moment of inertia.

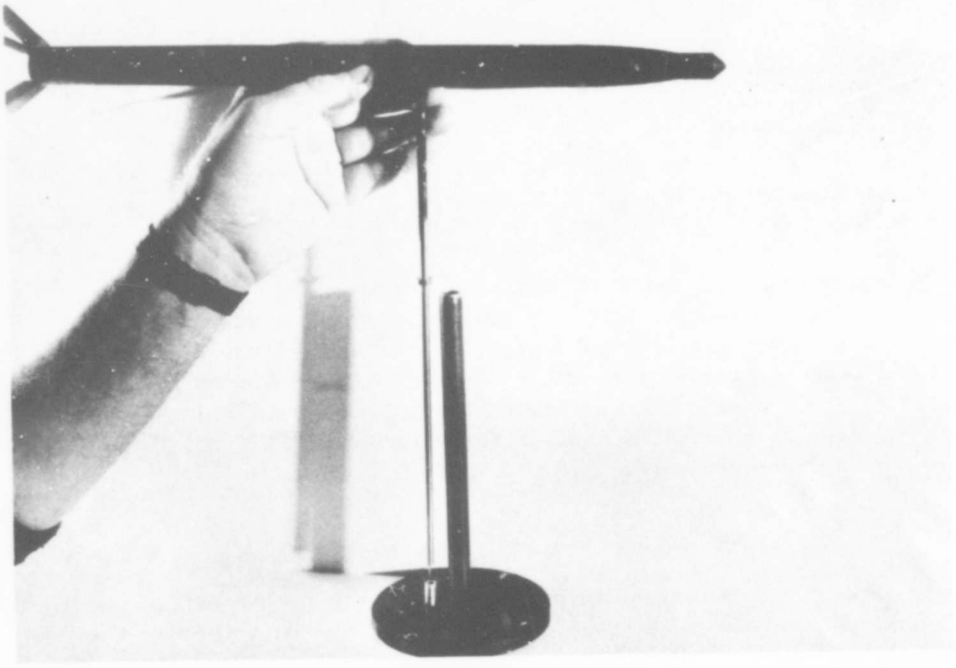

Figure 5. Model and Support System.

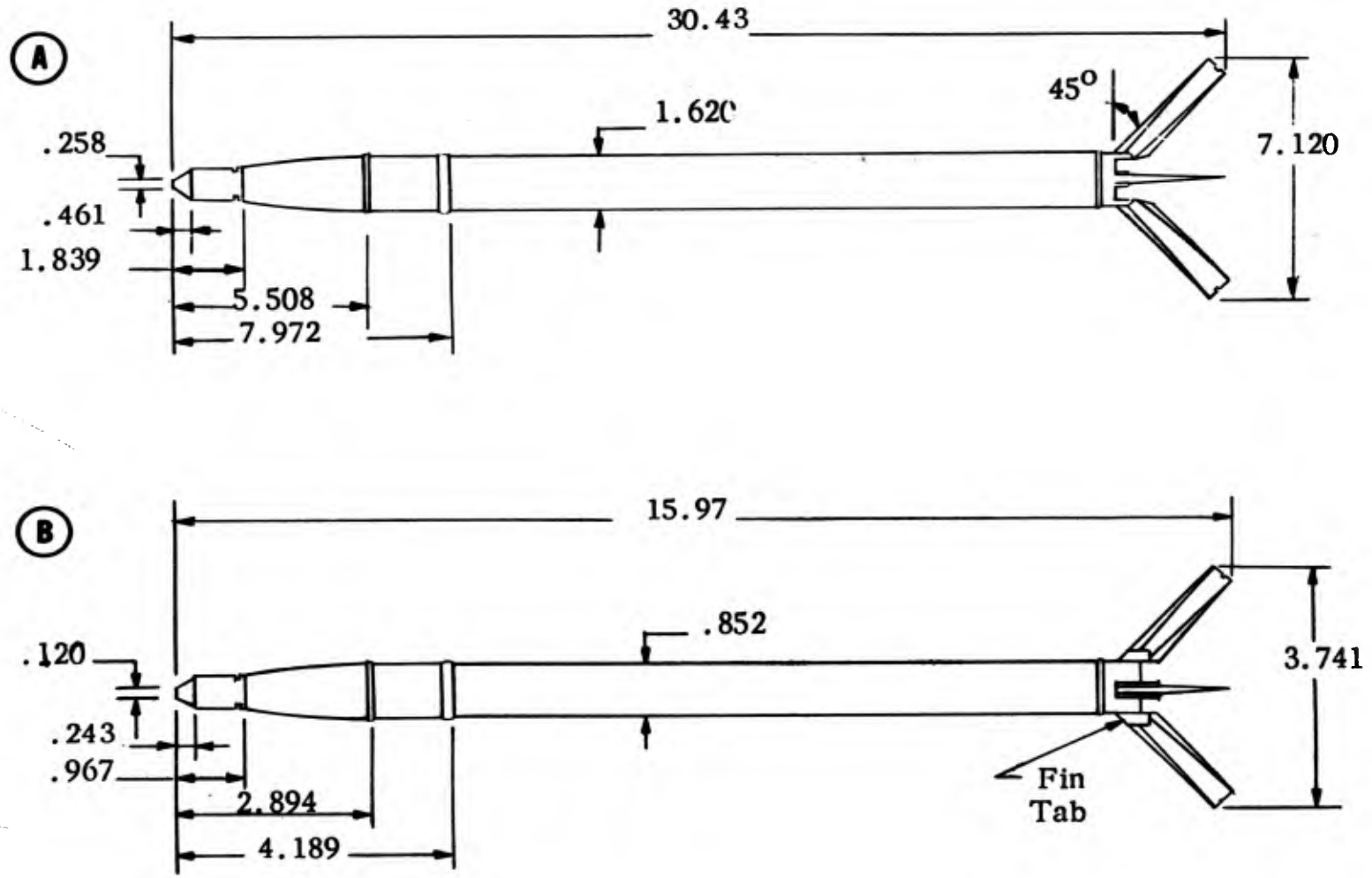

Figure 6. Test Facilities (A) .59-Scale Model Used in 40-Inch Supersonic Test Facility, and (B) .31-Scale Models Used in Notre Dame's 24-Inch Subsonic Test Facility and the One-Foot Transonic Test Facility at AEDC.

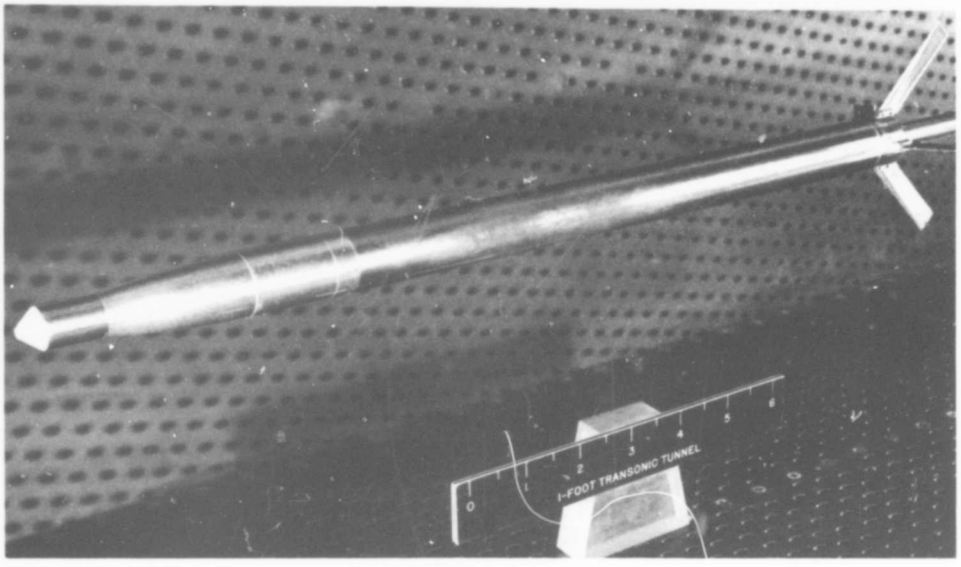

Figure 7. Model Installation in One-Foot Transonic Wind Tunnel.

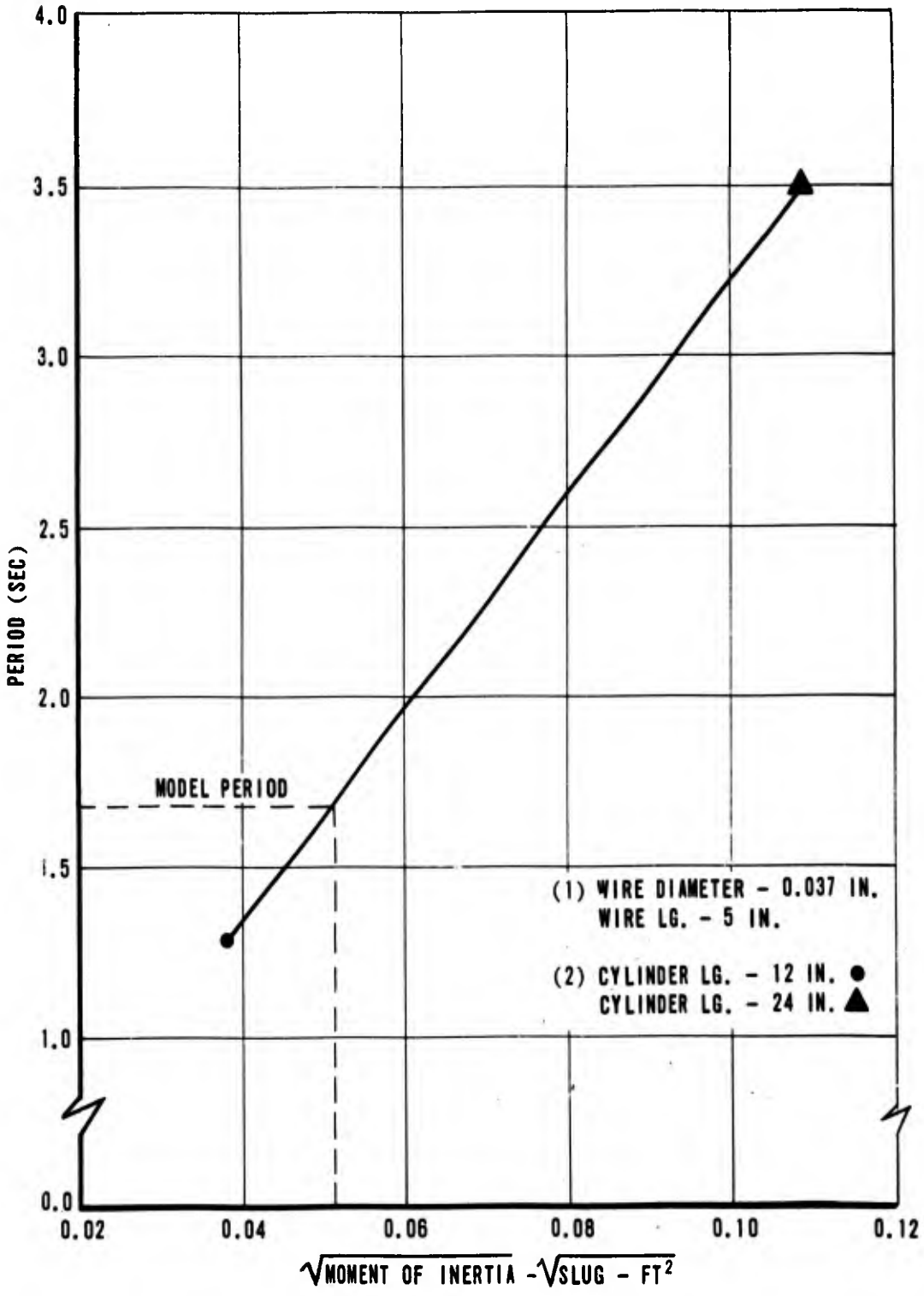

Figure 8. Model Moment of Inertia.

SINGLE DEGREE OF FREEDOM EXPERIMENTAL TECHNIQUE

Given period (T) and damping factor (λ) the stability coefficients C_{m_α} and C_{m_q} can be determined directly from the measured pitching motion, Ref. 1.

$$C_{m_\alpha} = - \frac{I \left[\frac{2\pi}{T}\right]^2}{1/2 \rho U^2 Sd}$$

$$C_{m_q} = \frac{2 I \lambda}{1/4 \rho USd^2}$$

The T and λ terms were determined from film using a mirror system as shown in Figure 2. The camera was mounted on a motorized cart which moves slowly while the lens remains open for a time exposure. The model was painted black with a small ball bearing attached to the forebody. The strobe provides pulses at a rate of 600 pulses per minute. The light reflection from the bearing provides a good reference mark for data reduction purposes.

The test procedure was to manually deflect the model, then with strobe operating and cart moving the lens was retained open until the motion damps to small amplitudes. A typical time history for the model is shown in Figure 9.

In order to obtain scale in the photographic plane reference marks are shown in the upper portion of Figure 9. The reference marks consist of two etched marks on a slender rod painted black which is inserted through the test section side wall.

The film is then read on a digital optical comparator, and a picture count reading is obtained for each strobe pulse by measuring the displacement of the bearing.

These raw data were converted to angular displacement when reduced to the UNIVAC 1107 "Wobble" computer program. This program fits the following equation to the data.

$$\alpha = \alpha_T + Ke^{\lambda t} \cos (\omega t + \delta)$$

In general a cruve procedure is accomplished by selecting a functional form which is either an exact or approximate solution of the differential equation. The parameters in the solution are adjusted to best fit the data. The method of least squares requires that the functions must be linear in the parameters, thus it is required to use the Method of Differential Corrections for the fitting process.

The Method of Differential Corrections has been used for a number of years by ballisticians to account for abnormal disturbances which are relatively small, such as wind effect and changes in density (Ref. 7).

The Method of Differential Corrections is used in the present analysis to fit the Tricycle Theory to the experimental data. A description of the use of the Method of Differential Corrections is given in Ref. 2 for the single degree of freedom case.

The problem is essentially to determine the values of α, t, K, λ, ω, and δ to be used in the classical expression shown above for single degree of freedom motion which best represents the motion for a given measured array of α versus time.

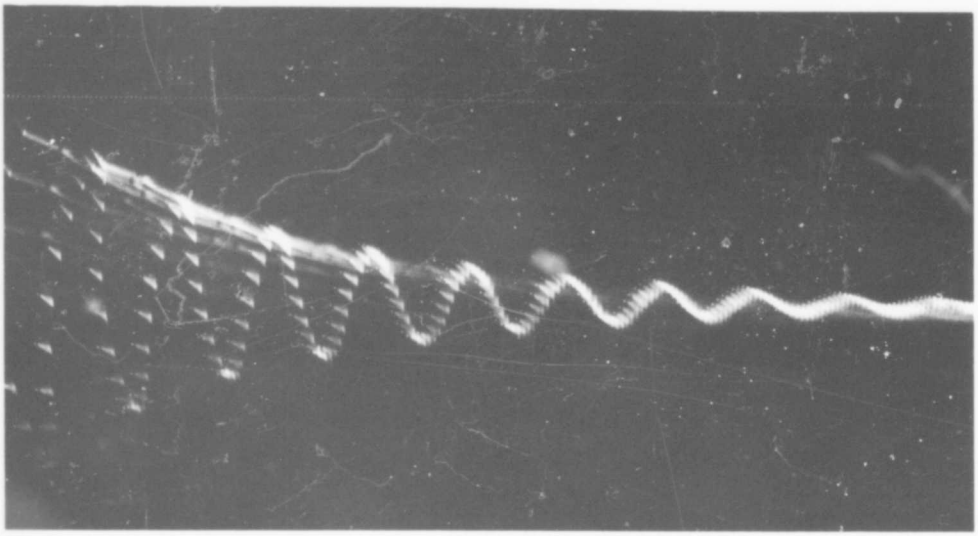

Fig. 9 TYPICAL RAW DATA

THEORY AND ANALYSIS UTILIZING "WOBBLE"

LINEAR MODEL

The Linear Theory of Nicolaides (Ref. 1) is presented for the linear model in a pure pitching mode with the center of gravity restrained. A nonlinear model will then be developed. The X, Y coordinate systems shown in Figure 10 are the vehicle principal axes systems and these axes rotate with the vehicle, whereas the x, y axes system is spaced fixed. Also shown in Figure 10 are the static and dynamic forces and moments which are considered acting on the body. These forces and moments in stability derivatives or aerodynamic stability coefficient form are:

$Z_\alpha \alpha = C_{Z_\alpha} \alpha Qs$ — Normal force in Z direction due to angle of attack (α).

$Z_q q = C_{Z_{\left[\frac{qd}{2V}\right]}} \frac{qd}{2V} QS$ — Normal force in Z direction due to pitching velocity (q).

$Z_{\dot\alpha} \dot\alpha = C_{Z_{\left[\frac{\dot\alpha d}{2V}\right]}} \frac{\dot\alpha d}{2V} QS$ — Normal force in Z direction due to rate of change of angle of attack ($\dot\alpha$).

$Z_{\delta_\epsilon} \delta_\epsilon = C_{Z_{\delta_\epsilon}} \delta_\epsilon QS$ — Normal force in Z direction due to fin or body asymmetries (δ_ϵ).

$M_\alpha \alpha = C_{m_\alpha} QSd$ — Moment about Y axis due to angle of attack (α).

$M_q q = C_{m_{\frac{qd}{2V}}} \frac{qd}{2V} QSd$ — Moment about Y axis due to pitching velocity (q).

$M_{\dot\alpha} \dot\alpha = C_{m_{\left[\frac{\dot\alpha d}{2V}\right]}} \frac{\dot\alpha d}{2V} QSd$ — Moment about Y axis due to rate of change of angle of attack ($\dot\alpha$).

$M_{\delta_\epsilon \delta_\epsilon} = C_{m_{\delta_\epsilon}} \delta_\epsilon QSd$ Moment about Y axis due to fin or body asymmetries (δ_ϵ).

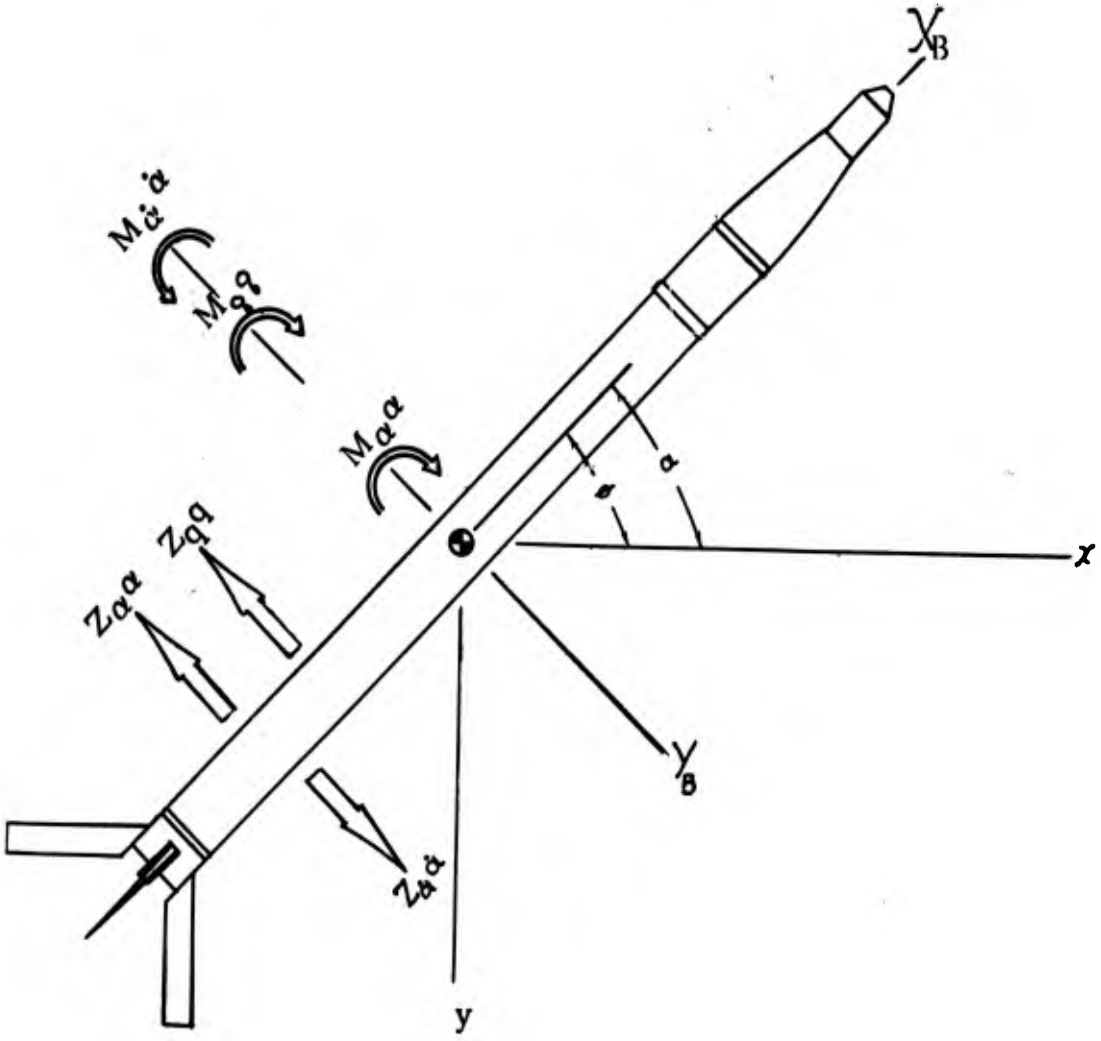

Figure 10. Static and Dynamic Forces and Moments Considered in Single Degree of Freedom Oscillation Tests.

In all cases, the body cross sectional area is used as the reference area (S) for the body diameter as the reference length (d). Newton's law for angular motion is given as

$$M = I \ddot{\theta} = M_\alpha \alpha + M_q q + M_{\dot{\alpha}} \dot{\alpha} + M_{\delta_\epsilon} \delta_\epsilon \qquad (1)$$

Since the model center of gravity is constrained, the pitch angle is identical to the angle of attack, thus

$$\theta = \alpha \text{ and } q = \dot{\theta} = \dot{\alpha}$$

Substituting the above into equation (1) yields

$$\ddot{\alpha} = \frac{M_{\alpha}\,\alpha}{I} + \frac{(M_q + M_{\dot{\alpha}})\dot{\alpha}}{I} + \frac{M_{\delta_e}\,\delta_e}{I}$$

which can be shown as

$$\ddot{\alpha} + N_1\,\dot{\alpha} + N_2\,\alpha = N_3 \qquad (2)$$

where

$$N_1 = -\frac{M_q + M_{\dot{\alpha}}}{I}$$

$$N_2 = -\frac{M_{\alpha}}{I}$$

$$N_3 = \frac{M_{\delta_e}\,\delta_e}{I}$$

Classical techniques are used for the solution of equation (2) which is a nonhomogeneous second order differential equation. Assuming a solution of the form $\alpha = Ke^{\varphi t}$ for the homogeneous solution yields

$$\alpha_H = K_1 e^{\varphi_1 t} + K_2 e^{\varphi_2 t}$$

where

$$\varphi_1 = -\frac{N_1}{2} + \frac{1}{2}\sqrt{N_1^2 - 4\,N_2} = \lambda_1 + i\omega_1$$

$$\varphi_2 = -\frac{N_1}{2} - \frac{1}{2}\sqrt{N_1^2 - 4\,N_2} = \lambda_2 + i\,\omega_2$$

Then assuming a solution of form $\alpha_p = K_3$ for the particular solution yields

$$\alpha_p = \frac{N_3}{N_2}$$

Now combining the above solutions

$$\alpha = K_1 e^{(\lambda_1 + i\omega_1)t} + K_2 e^{(\lambda_2 + i\omega_2)t} + K_3 \qquad (3)$$

Where K_1 and K_2 depend on the initial angle of attack and initial rate of change of angle of attack (α_0, $\dot{\alpha}_0$) or

$$K_1 = \frac{\dot{\alpha}_0 - \varphi_2 (\alpha_0 - K_3)}{\varphi_1 - \varphi_2}$$

$$K_2 = \frac{\dot{\alpha}_0 - \varphi_1 (\alpha_0 - K_3)}{\varphi_2 - \varphi_1}$$

$$K_3 = \frac{N_3}{N_2} \text{ Trim angle } (\alpha_t) \qquad (4)$$

Equation (3) may also be shown in the following form

$$\alpha = \alpha_T + Ke^{\lambda t} \cos(\omega t + \delta) \qquad (5)$$

The above expression is developed from equation (3) readily by assuming undamped motion.

$$\lambda_1 = \lambda_2 = 0 = \lambda \text{ and } \omega_2 = -\omega_1$$

Equation (3) may be shown as

$$\alpha = K_1 e^{i\omega_1 t} + K_2 e^{i\omega_2 t} + K_3 \qquad (6)$$

$$K_1 e^{i\omega_1 t} + K_2 e^{-i\omega_2 t} = K_1 \cos \omega_1 t + K_1 i \sin \omega_1 t + K_2 \cos \omega_1 t - i K_2 \sin \omega_1 t$$

$$= (K_1 + K_2) \cos \omega_1 t + i (K_1 - K_2) \sin \omega_1 t$$

Now let $A = K_1 + K_2$

$$B = i(K_1 - K_2)$$

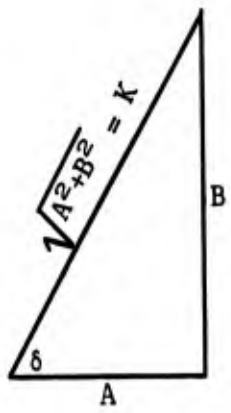

$$= A \cos \omega_1 t + B \sin \omega_1 t$$

$$\sin \delta = \frac{B}{\sqrt{A^2+B^2}} \qquad B = \sin \delta \sqrt{A^2+B^2}$$

$$\cos \delta = \frac{A}{\sqrt{A^2+B^2}} \qquad A = \cos \delta \sqrt{A^2+B^2}$$

Substituting A and B into the previous expression yields

$$\alpha = \sqrt{A^2+B^2}[\cos \delta \cos \omega_1 t + \sin \delta \sin \omega_1 t]$$

$$= \sqrt{A^2+B^2} \cos (\omega_1 t + \delta) \qquad (6a)$$

Now expanding the terms under the radical and substituting the following form of the K_1 and K_2 expression from equation (5)

$$K_1 = \frac{\dot{\alpha}_o + i\omega_1 \alpha_o}{2i\omega_1} = \frac{\dot{\alpha}_o i - \omega_1 \alpha_o}{-2\omega_1} = \frac{-\dot{\alpha}_o i + \omega_1 \alpha_o}{2\omega_1}$$

$$K_2 = \frac{\dot{\alpha}_o - i\omega_1 \alpha_o}{-2i\omega_1} = \frac{\dot{\alpha}_o i + \omega_1 \alpha_o}{2\omega_1}$$

$$A = K_1 + K_2 = \alpha_o \qquad B = i (K_1 - K_2) = i\left[\frac{-2\dot{\alpha}_o i}{2\omega_1}\right] = \frac{+\dot{\alpha}_o}{\omega_1}$$

$$A^2 = \alpha_o^2 \qquad B^2 = \frac{\dot{\alpha}_o^2}{\omega_1^2}$$

$$\sqrt{A^2+B^2} = \sqrt{\alpha_o^2 + \frac{\dot{\alpha}_o^2}{\omega_1^2}} \quad \text{and} \quad \delta = \tan^{-1} + \frac{\dot{\alpha}_o}{\omega_1 \alpha_o}$$

where α_o and $\dot{\alpha}_o$ are initial angular position and angular rate, and K, as used in equation (6), above, is defined as $K = \sqrt{\alpha_o^2 + \frac{\dot{\alpha}_o^2}{\omega_1^2}} = \sqrt{A^2+B^2}$

$\alpha = K \cos(\omega t + \delta)$ from equation (6a). Now adding asymmetry and damping terms

Thus $\alpha = \alpha_T + Ke^{\lambda t} \cos(\omega t + \delta)$

where $\alpha_T = \frac{N_3}{N_2}$ (trim angle due to fin or body asymmetries).

$\lambda = -\frac{N_1}{2}$ Viscous damping factor

$i\omega = 1/2\sqrt{N_1^2 - 4N_2} \approx \sqrt{-N_2}$ Circular frequency

δ = Phase angle or angle between time zero and the preceding positive maximum

$$N_1 = -C_{m_q} \frac{d}{2V} \frac{QSd}{I} \qquad N_2 = -C_{m_\alpha} \frac{QSd}{I}$$

The coefficients C_{m_α} and C_{m_q} are functions of ω and λ, respectively, and substituting the above expressions for ω and λ into the N_1 and N_2 expressions yield

$$C_{m_\alpha} = -\omega^2 \frac{I}{QSd} \qquad C_{m_q} = \frac{\lambda 4IV}{QSd^2}$$

where C_{m_q} is defined in this report as $C_{m_q} + C_{m_{\dot{\alpha}}}$.

NONLINEAR MODEL

Since actual motion is seldom linear, the previous linear Tricyclic Theory would not represent the motion for cases where ω and λ were not constants. ω and λ will vary with changing dynamic pressure and/or angle of attack, but only those variations due to angle of attack were considered in this report, since all tunnel test conditions were restricted to steady state dynamic pressures.

Attempts to fit the linear model to nonlinear data would result in large deviations between actual and fitted data as time progresses due to the changing frequency of the data and the assumed constant frequency used for the fitting process.

It is shown in Ref. 1 that the motion amplitude will change in the following manner when the motion frequency (ω) is changing.

$$K_t = K_o\sqrt{\frac{\omega_o}{\omega}}$$

Where K_o = Amplitude at time zero

ω_o = Frequency at time zero

Equation (6) can now be given as

$$\alpha = \alpha_T + K\sqrt{\frac{\omega_o}{\omega}}\, e^{\lambda t} \cos(\theta + \delta) \text{ where } \theta = \int_o^t \omega\, dt \qquad (7)$$

The ω term in equation (6) is given by a fourth degree polynomial which is obtained by fitting the polynomial to an array of ω versus time. The ω versus time array is obtained by assuming a linear model, and will be further discussed in the "Wobble" subroutine A 100.

In general, the technique is summarized below. The raw data shown in Figure 9 is converted to angular displacement (α) versus time. An approximation subroutine (APRXC) was then used to obtain initial estimates of α_T, ω, δ, K, and λ. These initial approximations are then used in the

fitting subroutine (A 100) to obtain improved values of α_T, ω, δ, K, and λ by successive fittings of sections of data. Although a linear model is assumed over each section of data fitted, the end result is an array of varying frequency with time since the section fits are incremented at small time intervals and represent a mean ω for that section. This array of ω versus time from the A 100 subroutine is then represented by fitting a fourth degree polynomial to the array of ω versus time using the A 100V subroutine. The polynomial in ω is then integrated to obtain φ. The polynomials for φ and ω are then used in equation (6) and again the Method of Differential Corrections is used to obtain final values of α_T, K, λ, ω_b, and δ. C_{m_α} and C_{m_q} at this point are given as a function of the maximum amplitude. In order to relate these coefficients to angle of attack, the subroutines CAQ(1) and CAQ(2) were used. Expressions for C_{m_α} and C_{m_q} as functions of angle of attack were then determined by second, fourth or sixth degree polynomials.

The subroutines of major interest noted above are discussed in more detail in the following pages.

"Wobble" fitting subroutines used in the single degree of freedom study are now discussed in some detail and also the subroutines relating C_{m_α} and C_{m_q} to angle of attack [Aprxc, A 100, A 100V, CAQ(1), CAQ(2)].

SUBROUTINE FOR INITIAL APPROXIMATION (APRXC)

The Method of Differential Corrections requires that first approximations of α_T, ω, δ, K, and λ be available. These are the constants required in fitting the single degree of freedom pitching motion.

$$\alpha = \alpha_T + Ke^{\lambda t} \cos(\omega t+\delta).$$

These constants may be "read in" but normally it is much easier to use computed approximations from the raw data. There approximations are arrived at in the following manner.

(a) The trim angle α_T is simply the mean of the peak to peak amplitude at the minimum amplitude.

(b) The frequency is normally determined from the entire oscillatory time history and will generally be quite satisfactory, but for cases where frequency may be extremely nonlinear as is the case for the 2.75-inch FFAR large yaw study, the first approximations should be based on the first portion of the oscillatory motion, since the actual initial frequency would be more closely approximated.

The frequency (ω) is then determined from

$$\omega = \frac{(m-1)\pi}{tm}$$

m = Number of maxima and minima points, and t_m = Time interval between the first and last point.

(c) The phase angle (δ) is determined from

$\delta = 2\pi - \omega t_1$ if the first extreme point is positive.

$\delta = \pi - \omega t_1$ if the first extreme point is negative.

(d) K is determined at time zero from the intercept at t = 0 of envelope enclosing maximum peaks to the trim angle (α_T) line.

(e) $\lambda = 0$ will normally suffice.

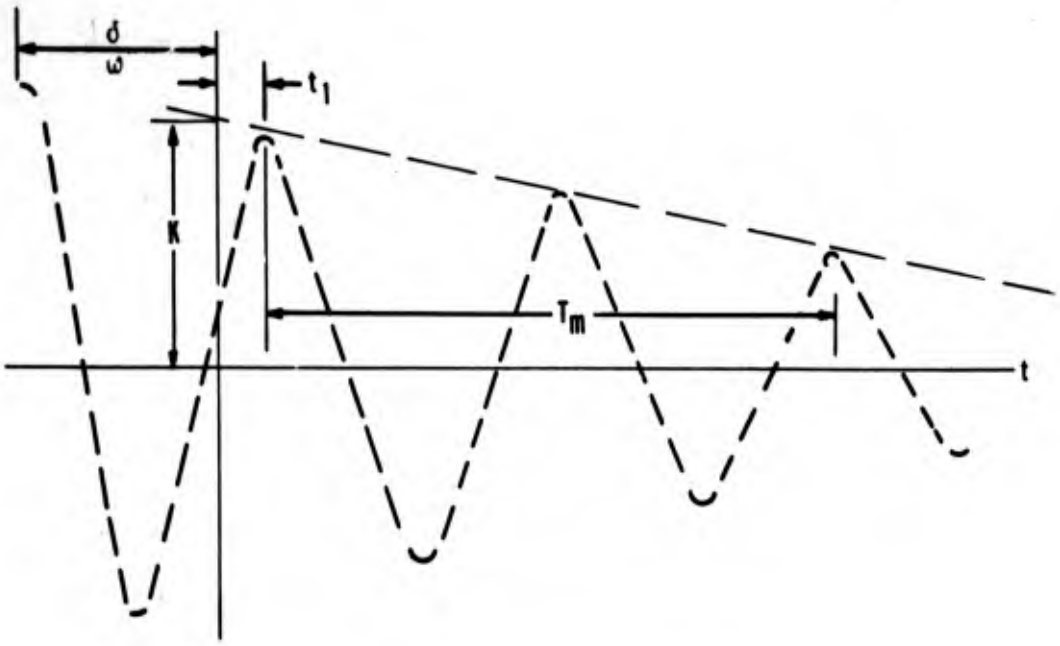
δ
ω
t_1
K
T_m
t

CONSTANT FREQUENCY FITTING SUBROUTINE (A1OO)

The A1OO subroutine utilizes the results of the APRXC subroutine or the first estimations of α_T, K, λ, ω and δ. This subroutine is then used to obtain improved values of α_T, K, λ, ω, and δ by a fitting process using the Method of Differential Corrections. Segments of data are fitted over segment lengths selected by considering the degree of nonlinear nature of data. For these test data, 1.5 cycles were used as the segment length due to large angles of attack and associated relatively large nonlinearities. Comparisons of pitch residuals were made for 1.5-, 2.0-, and 2.5-cycle segments and the residuals for the 1.5-cycle case were considerably lower than those observed for the 2.0- or 2.5-cycle case. Longer segments would normally be used for more linear data. In the fitting process up to 15 iterations are possible in arriving at the best fit but generally only four to six iterations are required. It should be noted that when using this subroutine the pitch residuals are a maximum initially and also at the end of the data where oscillations have decreased to a small amplitude. This is the result of the oscillation frequency not being constant as the motion damps. This variation in frequency is considered in the A1OOV "Wobble" subroutine.

VARIABLE FREQUENCY FITTING SUBROUTINE (A100V)

The A100V subroutine accounts for the variation in frequency at large and small angles of attack; otherwise, this subroutine is identical to A100. A comparison of pitch residuals from A100V and A100 indicated much smaller pitch residuals result when using the A100V subroutine. This improvement would not be so marked for cases in which the oscillation frequency did not vary significantly. A fourth degree polynomial is used to represent the varying oscillation frequency. This equation is

$$\omega(T) = C_0 + C_1 T + C_2 T^2 + C_3 T^3 + C_4 T^4$$

Sectional fits using the differential corrections method was previously used by A100 to determine ω and the other parameters. The frequency array which was determined from A100 is then represented by the above fourth degree polynomial whose coefficients are determined by a least squares fitting procedure. Time (T) as used in the above equation corresponds to the first value of ω. It is necessary that time be redefined in order to be given as the time from beginning of the section of data being fitted. Thus T in the above polynomial becomes $T = t_1$, where t_1 is the time from the beginning of the section, and on substitution into the above equation and expanding and collecting terms yields

$$\omega(t) = \omega_0 + C_1'(t) + C_2'(t)^2 + C_3' t^3 + C_4' t^4$$

where $C_n' = f(C_n, t_1)$

This equation is then integrated to obtain

$$\theta = \omega_0 t + \frac{C_1 t^2}{2} + \frac{C_2 t^3}{3} + \frac{C_3 t^4}{4} + \frac{C_4 t^5}{5}$$

where θ is then used in the following equation:

$$\alpha = \alpha_T + K\sqrt{\frac{\omega_0}{\omega}}\, e^{\lambda t} \cos(\theta + \delta)$$

The $\frac{\omega_0}{\omega}$ term accounts for the effect of varying frequency on the amplitude where ω is the frequency at the start of the data being fitted.

The method of Differential Corrections is then applied again to fit the above equation to the data to obtain α_T, K, λ, ω, and δ.

GENERAL COMMENTS ON FITTING TECHNIQUES

Although only A100 and the A100V fitting subroutines are used for the single degree of freedom case the other fitting subroutines are simply extensions of the technique used in the single degree of freedom technique. The following flow diamgram shown in Figure 11 is applicable to all fitting subroutines in "Wobble." The flow diagram is applicable to each section of data fitted. Each section of data was incremented dive data points or .5 second and a new section fit accomplished.

Eikenberry has recently shown that optimum section lengths of 1.3, 1.8, 2.3, 2.8, 3.3, and 3.8 that are desirable in order to reduce the scatter band in amplitude. When these scatter bands are examined in detail, it is found that the wave form will contain a second and fourth harmonic. These second and fourth harmonics result from the third harmonic which is added or subtracted to the basic frequency. The second harmonic should be approximately twice the amplitude of the fourth harmonic.

The origin of the scatter is in the changing relation between the end points of the section of data being fitted and the third harmonic. In reality the fifth harmonic would also be present, but the effect of this harmonic is apparently very small since corresponding amplitudes and frequency were not detectable in the scatter bands.

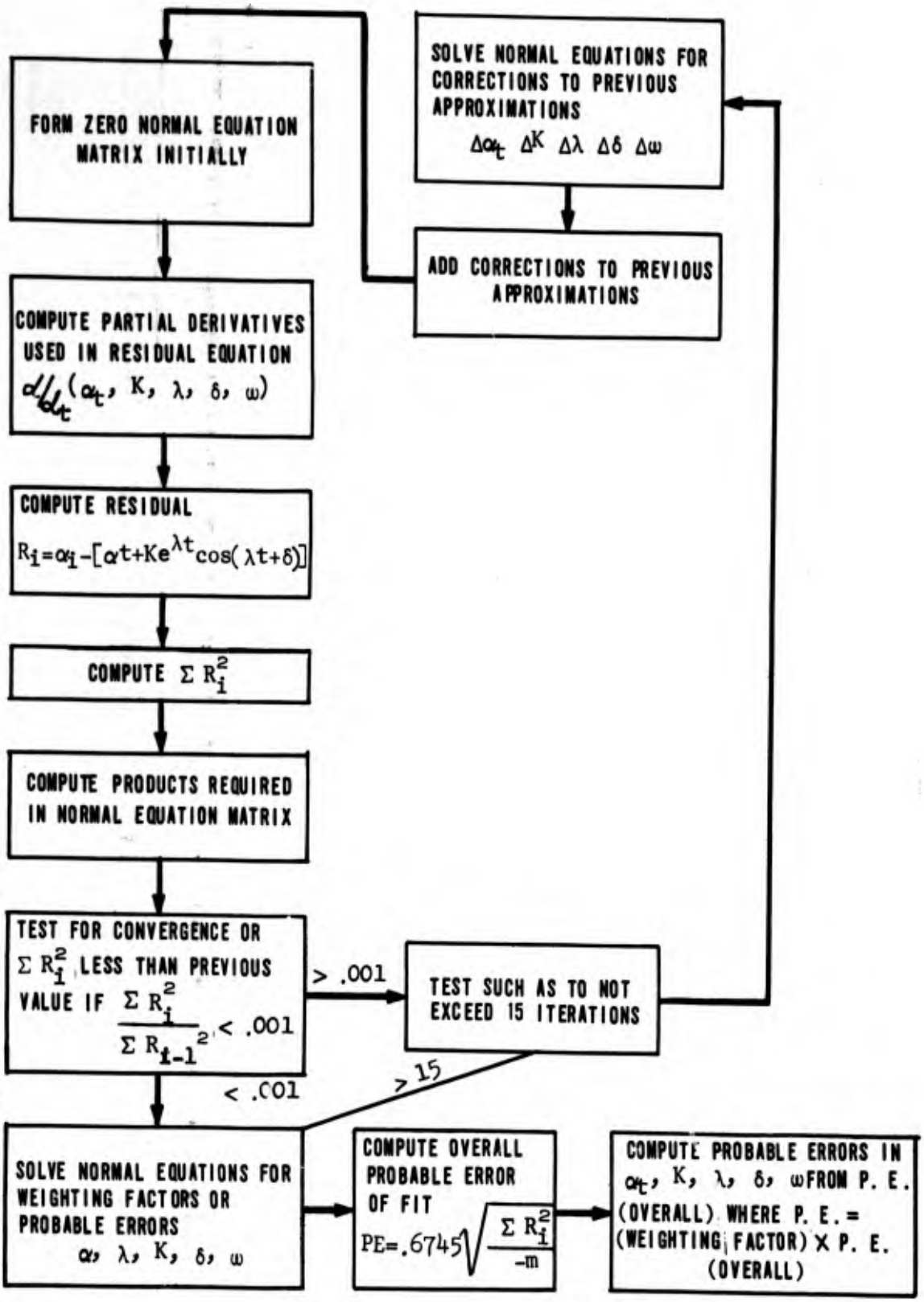

Figure 11. Flow Diagram for General Fitting Process.

DETERMINATION OF C_{m_α} AND C_{m_q} AS $f(\alpha)$ (CAQ SUBROUTINE)

A considerable number of data points are required for a particular section fit. Coefficients obtained from such a section fit represent mean values and are related to the maximum amplitude envelope rather than to the angle of attack since the instantaneous angle of attack recorded during the section fit was changing continuously. To be of practical value for use with trajectory predictions or similar computer studies, we must express the damping coefficient as a function of instant aneous angle of attack. This is essentially the sole purpose of the CAQ subroutines with the end product being a polynomial of selected degree to represent C_{m_q} and C_{m_α} as a function of angle of attack.

The method of Redd, Ref. 4, assumes a constant M_α or frequency to determine C_{m_q}. Redd's technique is therefore not applicable for cases where large nonlinearities in M_α or changes in ω are evident, unless Redd's technique is used in confunction with the A1OOV "Wobble" subroutine which accounts for the variations in frequency with amplitude.

Rasmussen has developed a more general approach which assumes nonlinearities in M_α and M_q and in general should provide the best results for cases where large angles of attack are considered. Ref. 3 describes the method used which assumes that the nonlinear portion of the damping term is small while at the same time allowing large nonlinearities in M_α. Eikenberry has shown that the technique of Rasmussen's appears to provide very good results even for large non-linearities in M_α.

REDD TECHNIQUE

Redd, Ref. 4, presented a case for determining the pitch damping coefficient as a function of instantaneous angle of attack which assumes that C_{m_α} is linear and the damping per cycle is small. The development and equations used in the subject reference are described below.

A single degree system with damping and restoring moment is described by the following nonlinear differential equations for the forced and free oscillation techniques, respectively.

$$I\ddot{\alpha} + f(\alpha)\,\dot{\alpha} + k\,\alpha = 0 \tag{8}$$

$$I\ddot{\alpha} + f(K)\,\dot{\alpha} + k\,\alpha = 0 \tag{9}$$

and f(K) represents M_q as a function of instantaneous angle of attack (α) and amplitude (K) respectively. Kryloff and Bogoliuboff (Ref. 8) have shown that the linear equation (9) is the equivalent form of the nonlinear equation (8). This equivalence is shown by noting that the work done during a forced oscillation is equivalent to that done during a free oscillation. This is shown in the following relationships:

Work for forced oscillation cycle = work for free oscillation cycle

or

$$\int_0^T f(\alpha)\,\dot{\alpha}^2\,dt = f(K) \int_0^T \dot{\alpha}^2\,dt \tag{10}$$

The average damping coefficient is then shown as

$$f(K) = \frac{\int_0^T f(\alpha)\,\dot{\alpha}^2\,dt}{\int_0^T \dot{\alpha}^2\,dt} \tag{11}$$

The f(K) and f(α) terms for mirror symmetry can be expressed as

$$f(\alpha) = A + A_2\,\alpha^2 + A_4\alpha^4 + A_6\alpha^6 + \ldots\ldots$$

$$f(K) = C + C_2K^2 + C_4K^4 + C_6K^6 + \ldots\ldots$$

Equation 11 is then rewritten as:

$$f(K) = C + C_2K^2 + C_4K^4 + C_6K^6 = \frac{\int_0^T (A+A_2\alpha^2+A_4\alpha^4+A_6\alpha^6)\dot{\alpha}^2 dt}{\int_0^T \dot{\alpha}^2 dt} \tag{12}$$

The damping moment is assumed small such that K can be considered constant over the cycle. Alpha (α) is then given by $\alpha = K \cos \omega t$ with

the assumption that a cosine wave would sufficiently represent the motion. This is the case although distortion of the wave form is apparent from the presence of the third harmonic. Substitutions for expression for $\dot{\alpha}$ and α into equation (12) yields

$$f(K) = \frac{\int_0^T (A+A_2\alpha^2\cos^2\omega t+A_4\alpha^4\cos^4\omega t+A_6\alpha^6\cos^6\omega t)\, K^2\omega^2\sin^2\omega t\, dt}{\int_0^T K^2\omega^2\sin^2\omega t} \qquad (13)$$

Equation (13) can now be integrated. The integration of the first few terms are shown below.

$$\frac{\int_0^T A\, K^2\, \omega^2\, \sin^2\omega t\, dt}{\int_0^T K^2\, \omega^2\, \sin^2\omega t} = A$$

$$\frac{\int_0^T (A_2\, K^2\cos^2\omega t)\,(K^2\omega^2\sin^2\omega t)\, dt}{\int_0^T K^2\, \omega^2\, \sin^2\omega t} = \frac{A_2 K^2}{4}$$

$$\frac{\int_0^T (A_4 K^4\cos^4\omega t)\,(K^2\omega^2\sin^2\omega t)\, dt}{\int_0^T K^2\, \omega^2\, \sin^2\omega t} = \frac{A_4\, K^4}{8}$$

$$\frac{\int_0^T (A_6 K^6\cos^6\omega t)\,(K^2\omega^2\sin^2\omega t)\, dt}{\int_0^T K^2\, \omega^2\, \sin^2 dt} = \frac{5A_6\, K^6}{64}$$

Equation (11) can now be shown as

$$C+C_2K^2+C_4K^4+C_6K^6 = A+\frac{A_2K^2}{4}+\frac{A_4K^4}{8}+\frac{5A_6K^6}{64}$$

Then equating like coefficients from equation (11) the following results:

Where $C = A$

$$C_2 = \frac{A_2}{4} \text{ or } A_2 = 4C_2$$

$$C_4 = \frac{A_4}{8} \text{ or } A_4 = C_4$$

$$C_6 = \frac{5A_6}{64} \text{ or } A_6 = \frac{64}{5}C_6$$

With f(K) known from the free oscillation data and expressed in the series form shown in equation (13), $f(\alpha)$ can then be determined directly from

$$f(\alpha) = C+4C_2\alpha^2 + C_4\alpha^4 + \frac{64}{5}C_6\alpha^6 \qquad (14)$$

the damping coefficient is then determined from

$$C_{m_q} = \frac{f(\alpha)}{\frac{qSD^2}{2V}}$$

The coefficients C, C_2, C_4, C_6 in equation (14) are determined from a least squares fit of an even order polynomial to C_{m_q} versus K, C_{m_q} may then be expressed as a power series.

$$C_{r_q} = \frac{\frac{1}{qSD^2}}{2V}\left[C+4C_2\alpha^2 + C_4\alpha^4 + \frac{64}{5}C_6\alpha^6\right] \qquad (15)$$

It is recommended that when using the Redd technique that in all cases this should be used in conjunction with A1OOV, to account for variations in frequency with amplitude. The Redd technique may be used to determine C_{m_q}, whereas the method by Rasmussen, Ref. 3, is applicable for obtaining $C_{m_{\dot{q}}}$ or $C_{m_{\dot{\alpha}}}$.

C_{m_α} BY RASMUSSEN TECHNIQUE

To alleviate the restriction of a linear C_{m_α} as is assumed in the Redd technique, the more recent work by Rasmussen may be used. This method has the advantage of considering nonlinearities in the static and damping moment. An approximate solution is obtained which assumes small damping but large nonlinearities in C_{m_α}.

The following technique for obtaining C_{m_α} is used in both CAQ(1) and CAQ(2) subroutines. Only these results used in the computer program will be presented. Details on the development of the equations used are given in Ref. 3 and 4.

C_{m_α} can be shown as an even order polynomial in amplitude (K) or angle of attack (α) as shown below:

$$C_{m_\alpha}(\alpha) = C_0 + C_2 \alpha^2 + C_4 \alpha^4 + C_6 \alpha^6$$

$$C_{m_\alpha}(K) = C_0' + C_2' K^2 + C_4' K^4 + C_6' K^6$$

The coefficients in the above equations are

$$C_n = \frac{C_n'}{A_n} \quad \text{where} \quad A_n = \frac{4}{n+2}\left[1 - (1/2)^{\frac{n+1}{2}}\right] \qquad n = 0,2,4,6$$

n	A_n	$C_n = C_n'/A_n$
2	.75	$1.3333C_n$
4	.5833	$1.7143C_n$
6	.4687	$2.1333C_n$

Thus $C_{m_\alpha} = C_o + 1.3330 C_n' \alpha^2 + 1.7143 C_n' \alpha^4 + 2.1333 C_n' \alpha^6$

C_n' is then found by a least squares fit of an even order polynomial to C_{m_α} versus K after which all terms required for C_{m_α} as a function of angle of attack have been obtained. It should be noted that higher degree polynomials can be obtained as required.

C_{m_q} BY RASMUSSEN TECHNIQUE

As previously noted the method of Redd used to determine C_{m_q} assumes a linear C_{m_α}. Rasmussen's technique is considerably more involved than the previous method since nonlinearities in C_{m_α} with angle of attack are considered. The development of the equations used is complex although the end result in the approximate solution form, results in simple relationships.

C_{m_q} can be shown as an even order polynomial in amplitude (K) with coefficients that are functions of the static pitch damping moment coefficient.

$$C_{m_q} + C_{m_{\dot\alpha}} = C_1B_1+C_2B_2K^2+C_3B_3K^4+C_4B_4K^6$$

where

$$B_n = \frac{1}{2n}\left[\frac{\alpha_{m_1}A_1+\alpha_{m_2}A_2K^2+\alpha_{m_3}A_3K^4+\alpha_{m_4}A_4K^6}{B_{m_1}A_1+B_{m_2}A_2K^2+B_{m_3}A_3K^4+B_{m_4}A_4K^6}\right]$$

The A terms are functions of the static pitching and pitch damping moment coefficients. In Ref. 3, the A terms are determined graphically and Eikenberry utilizes a least squares fit of C_{m_α} and C_{m_q} to obtain these terms.

C_{m_α} can be shown as an even order polynomial in amplitude (K) or angle of attack as shown below.

$$C_{m_\alpha}(\alpha) = A_1 + \frac{3}{4}A_2K^2 + \frac{7}{12}A_3K^4 + \frac{15}{32}A_4K^6$$

$$C_{m_\alpha}(K) = A_1' + A_2'K^2 + A_3'K^4 + A_4'K^6$$

The least squares fit determines the A_1', A_2' A_3' and A_4' terms which can then be related to A_1, A_2, A_3 and A_4 by the following:

$$A_1 = A_1'$$

$$A_2 = 4/3\ A_2'$$

$$A_3 = \frac{12}{7} A_3'$$

$$A_4 = \frac{32}{15} A_4'$$

The α_{m1}, α_{m2}, α_{m3}, α_{m4} and B_{m1}, B_{m2}, B_{m3}, B_{m4} terms are obtained from Ref. 3 and are shown in the following table.

	α_{mn}			
S	n=1	n=2	n=3	n=4
1	2.0000	1.0000	.7500	.6250
2	1.2500	.6797	.5250	.4428
3	.9167	.5213	.4118	.3519
4	.7266	.4249	.3415	.2950

	B_{mn}			
S	N=1	N=2	N=3	N=4
1	1.0000	1.0000	1.0000	1.0000
2	.9375	.9297	.9188	.9084
3	.9167	.9067	.8929	.8797
4	.9082	.8975	.8831	.8688

The subscripting used in the above table differs from that used in Ref. 3 by a factor of 2n-2 for convenience in programming.

It remains to determine the C terms in the C_{m_q} relationship. This is accomplished by a least squares fit of C_{m_q} versus K and it must be noted that in accomplishing this fit that B_n is a function of K. Therefore, the residual equations would have the following form,

$$\mathcal{L} v^2 = C_{m_q} - (C_1B_1+C_2B_2K^2+C_3B_3K^4+C_4B_4K^6)^2$$

$$\frac{\partial v^2}{\partial C_n} = -2\sum B_n K^{2n-2}\left[C_{m_q} - (C_1B_1+C_2B_2K^2+C_3B_3K^4+C_4B_4K^6)\right]$$

The normal equation symmetric matrix can then be shown as

$$\begin{bmatrix} B^2 & B_1B_2K^2 & B_1B_3K^4 & B_1B_4K^6 \\ & B_2{}^2K^4 & B_2B_3K^6 & B_2B_4K^8 \\ & & B_3{}^2K^8 & B_3B_4K^{10} \\ & & & B_4{}^2K^{12} \end{bmatrix} \begin{bmatrix} C_1 \\ C_2 \\ C_3 \\ C_4 \end{bmatrix} \quad \begin{bmatrix} B_1C_{m_q} \\ B_2K^2C_{m_q} \\ B_3K^4C_{m_q} \\ B_4K^6C_{m_q} \end{bmatrix}$$

DISCUSSION OF RESULTS

Data results from "Wobble" are presented in Tables I-VII and in Figures 12-22. Typical values of C_{m_α} and C_{m_q} as determined from the fitting process for successive sections are shown in Table V where the TI and TM refers to time at the beginning and middle of the particular section. The increment in time used for each successive section fit was .5 second. It is apparent from the data that with increasing time or decreasing amplitude that C_{m_α} and C_{m_q} are varying with amplitude and the nonlinear nature of these coefficients with angle of attack.

Table III shows the parameters $(\alpha, K, \lambda, \omega, \alpha)$ and their respective probable errors, which were obtained for successive section fit and a percentage error in K and ω. A mean percentage error in K and ω for all section fits for eight runs were .4417 and .0944, respectively. It is evident that the tricyclic theory represents the data quite well. Percentage errors for indivicual runs are shown in Table IV.

The probable error in various ordered polynomial expressions for the C_{m_α} and C_{m_q} residuals as f(K) are shown in Table VII for two of eight different runs. Run numbers 1-4 in general were accomplished with larger initial angles of attack where as run numbers 5-8 correspond to relatively small initial angles of attack. These probable errors represent an overall probable error which is computed from an array of C_{m_α} versus K and C_{m_q} versus K. These probable errors, although given for fitting a polynomial to C_{m_α} versus K, would also be indicative of the probable errors encountered when using the polynomials expressing C_{m_α} as $f(\alpha)$ shown in Table IV, since CAQ(1) is used and the polynomials for C_{m_α} or C_{m_q} as a function of K or α differ only by a constant in the even ordered terms. The determination of C_{m_α} appears to be considerably better than C_{m_q}. This can be shown by Table V by comparing the percentage errors in C_{m_α} and C_{m_q} at small angles of attack would indicate approximately 2 and 16 percent, respectively, for any given run.

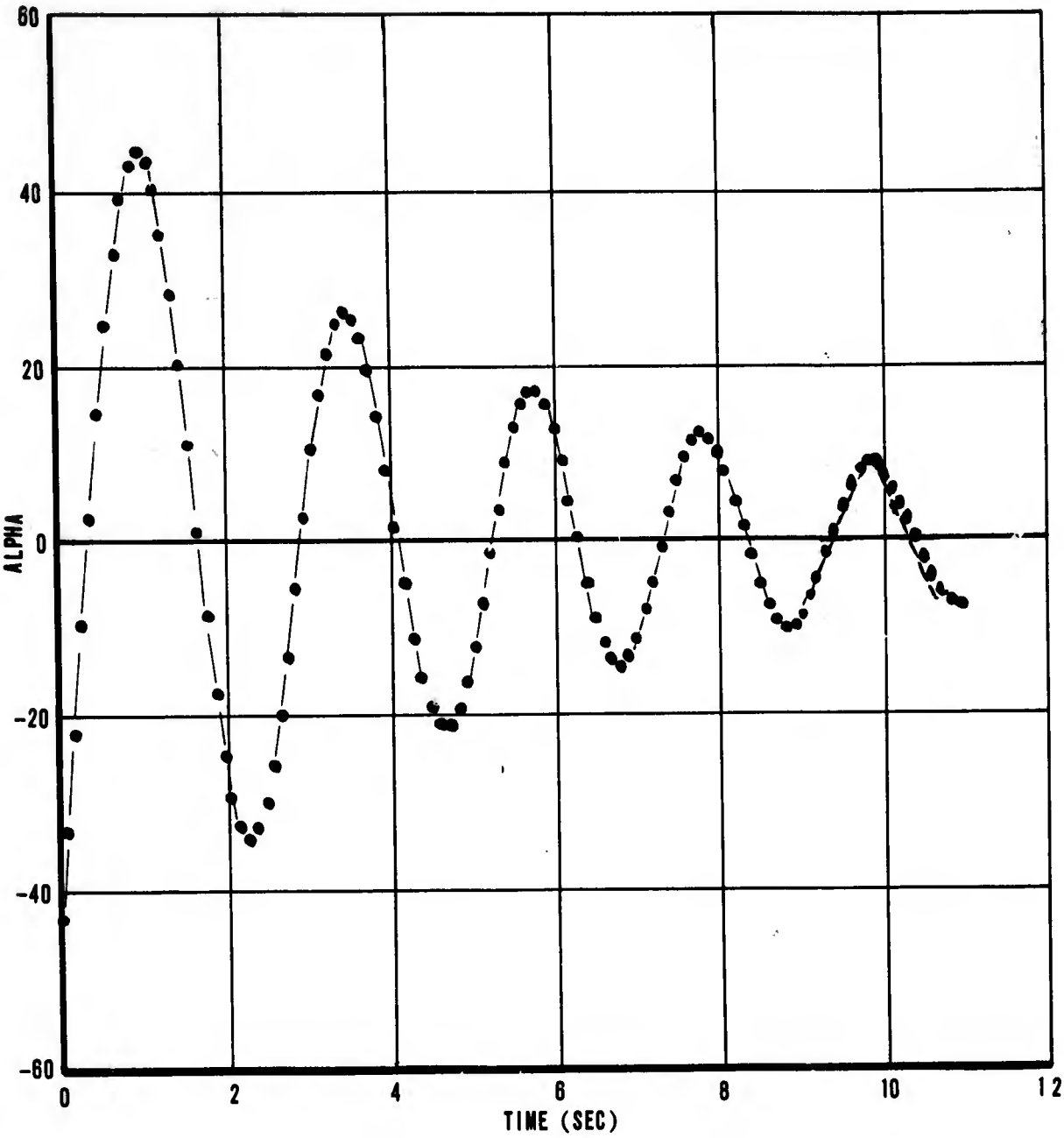

Figure 12. Variation of Angle of Attack With Time (Run Number 1).

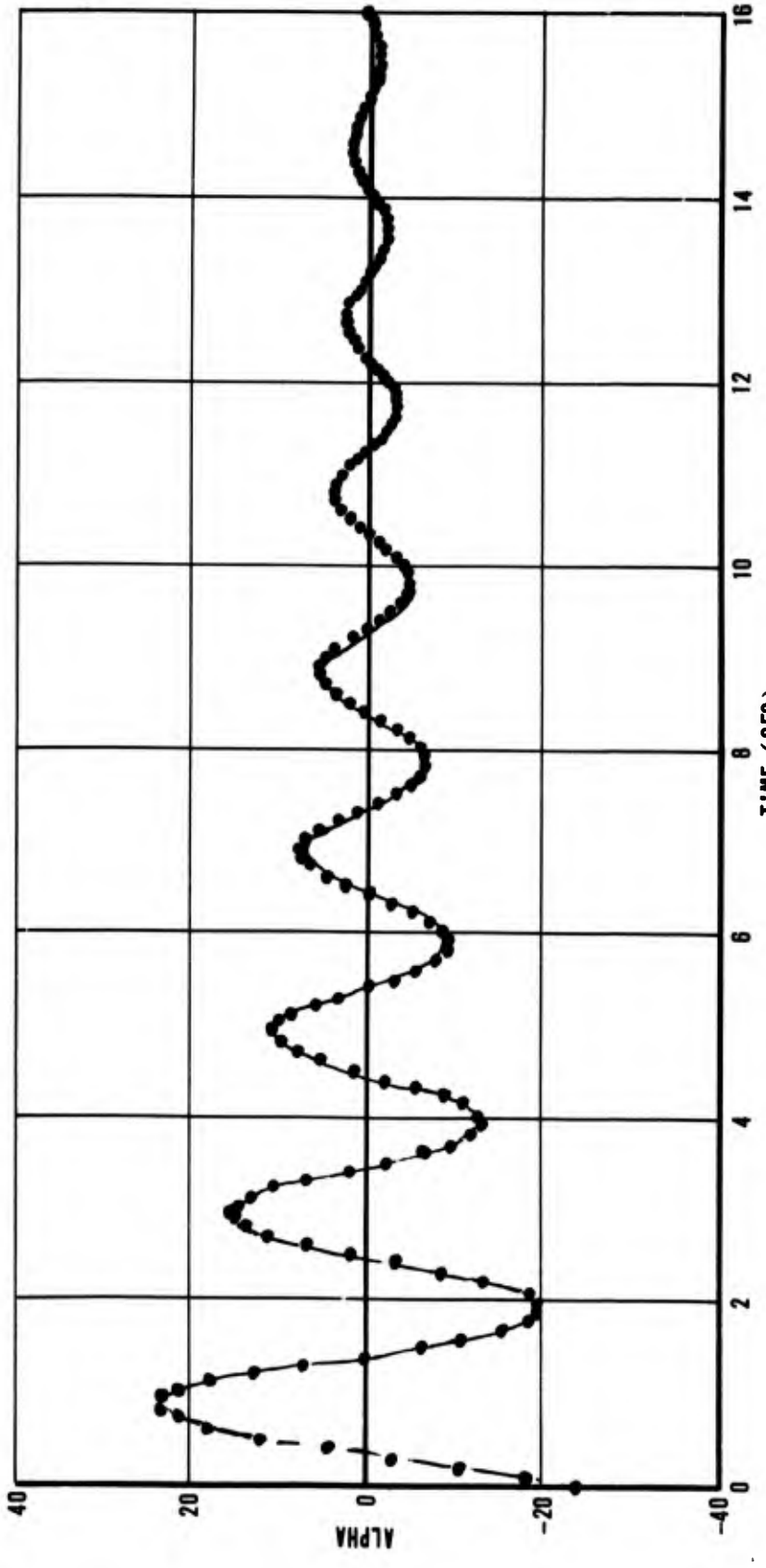

Figure 13. Variation of Angle of Attack With Time (Run Number 6).

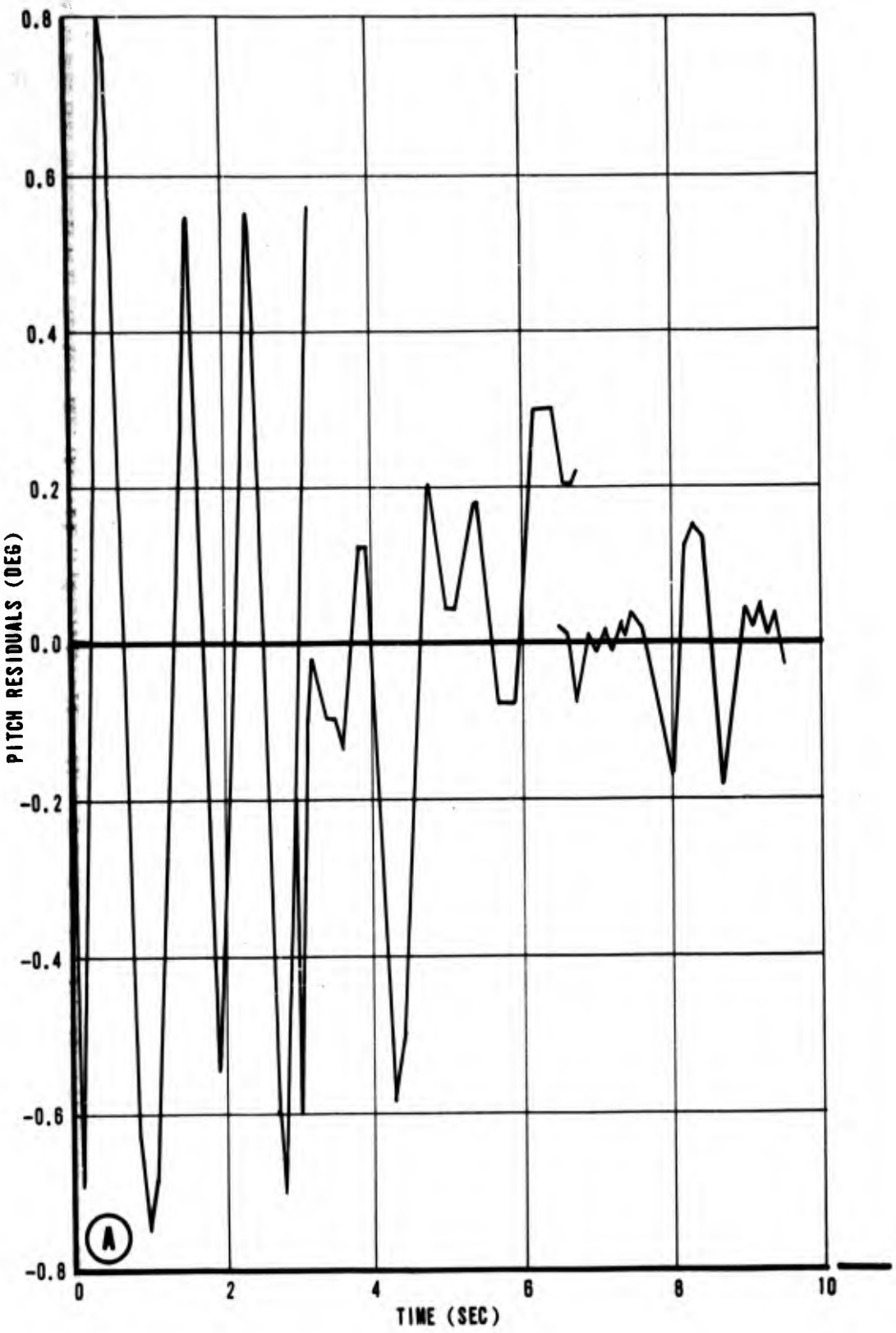

Figure 14(a). Variation of Pitch Residuals Versus Time (Run Number 1).

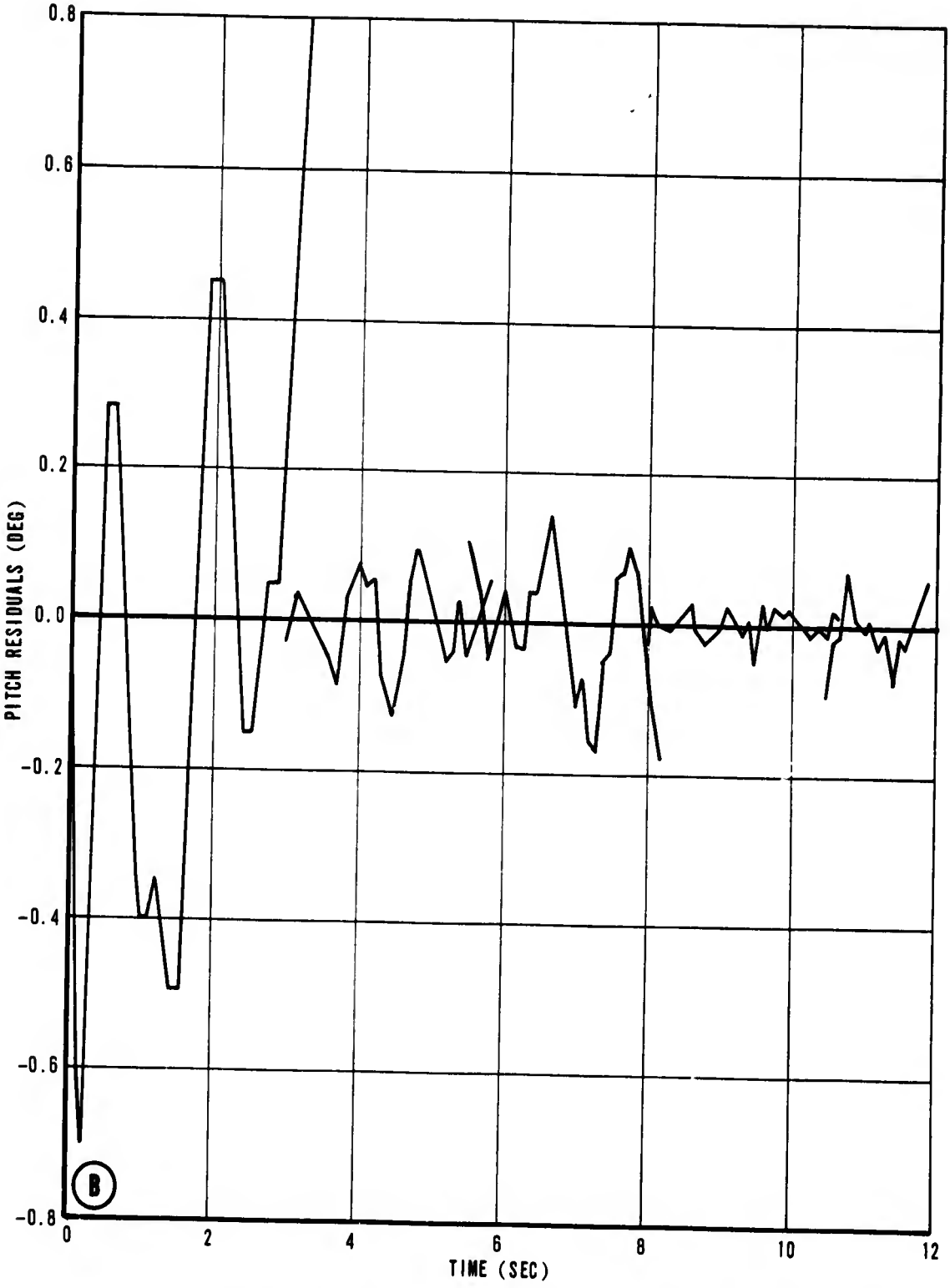

Figure 14(b). Variation of Pitch Residuals Versus Time (Run Number 6).

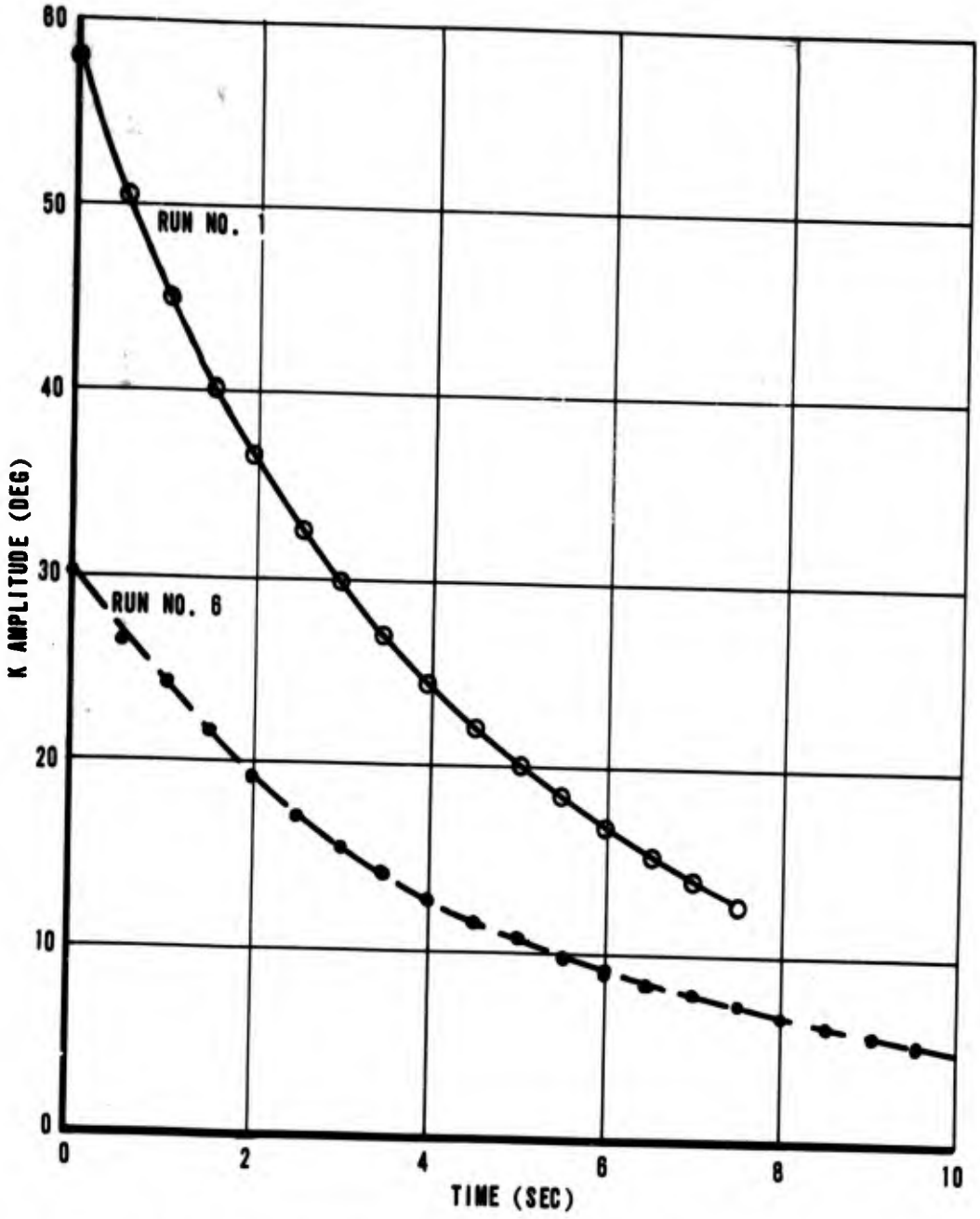

Figure 15. Variation of K Amplitude With Time.

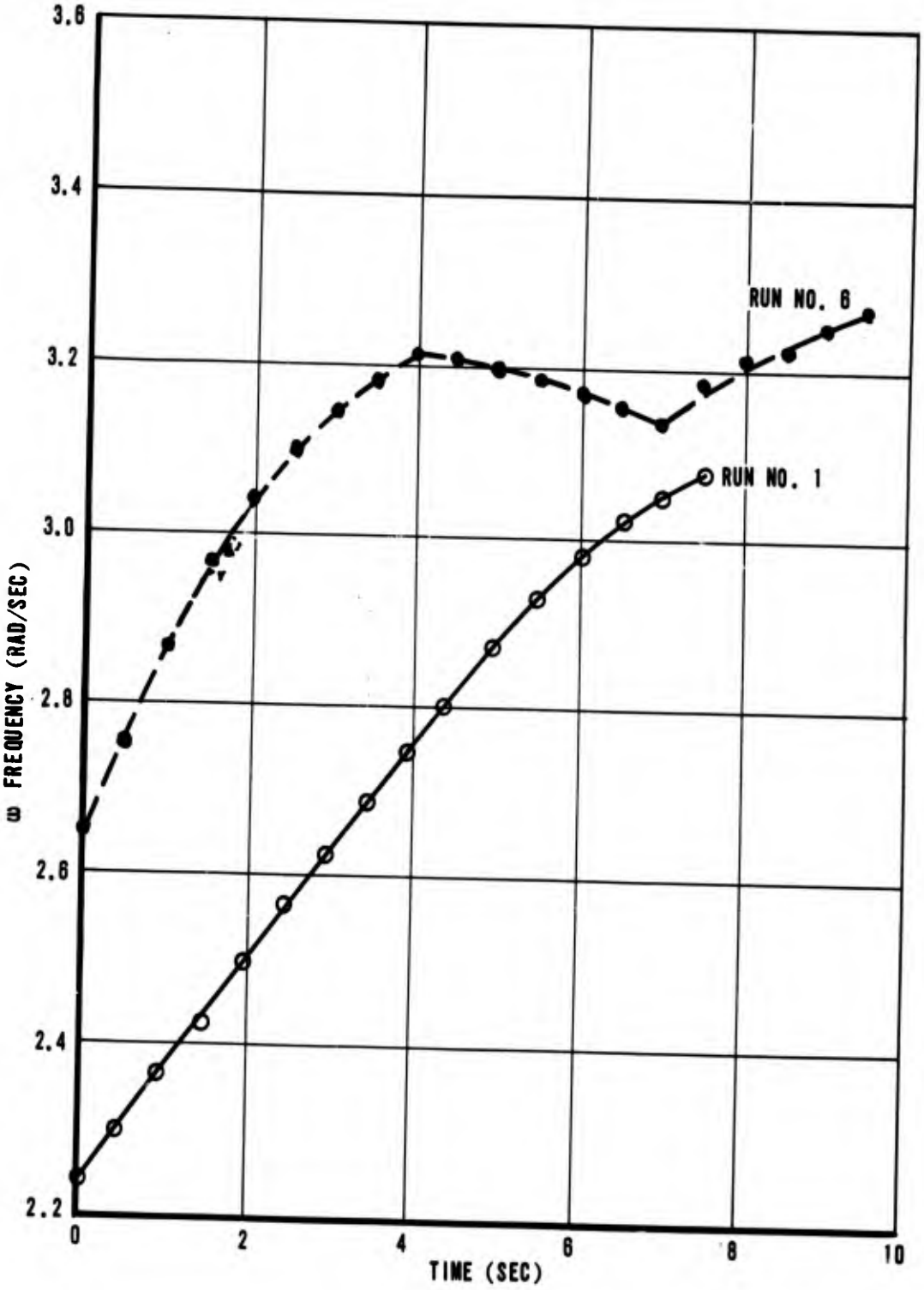

Figure 16. Variation of Frequency With Time.

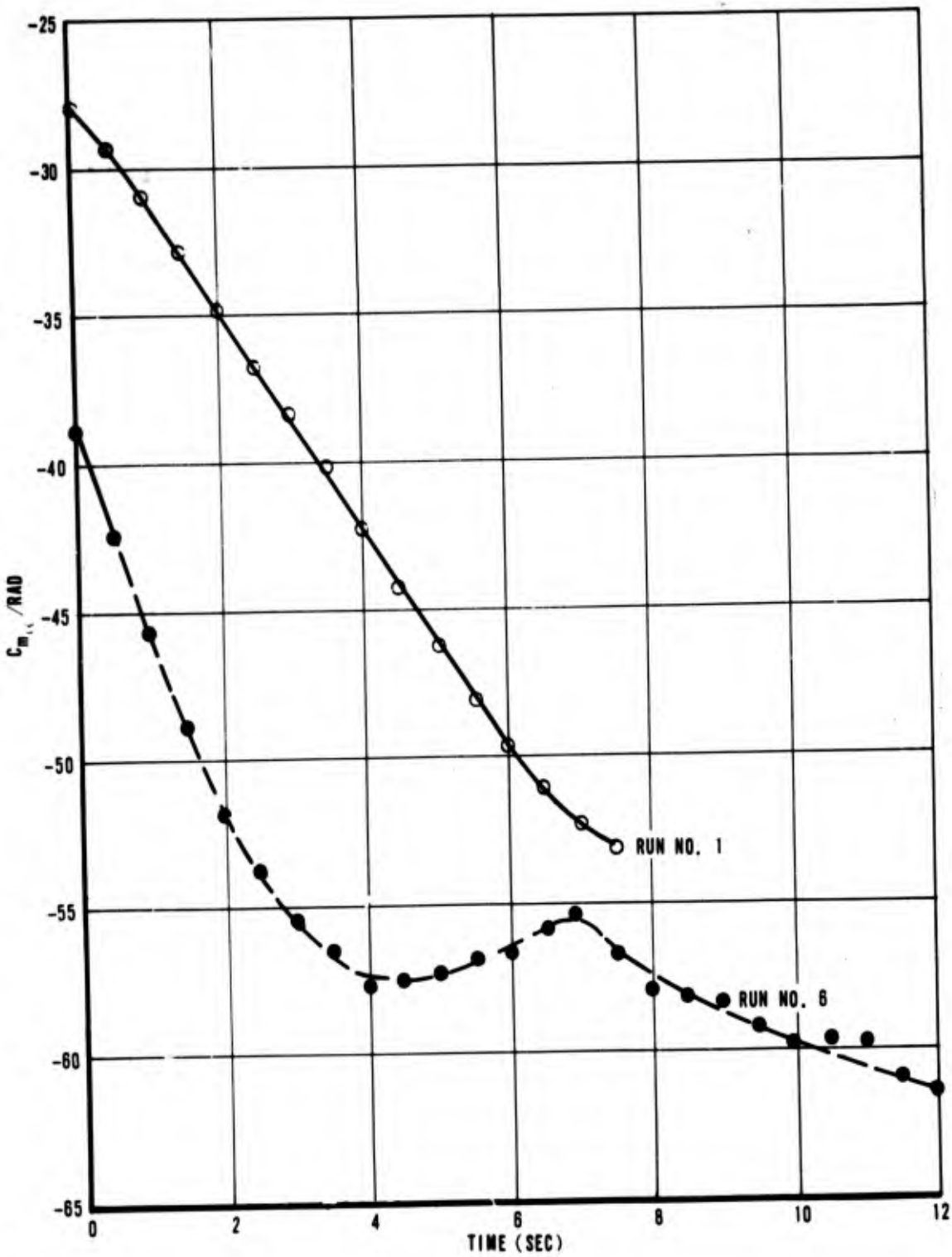

Figure 17. Variation of Static Pitching Moment Curve Slope With Time.

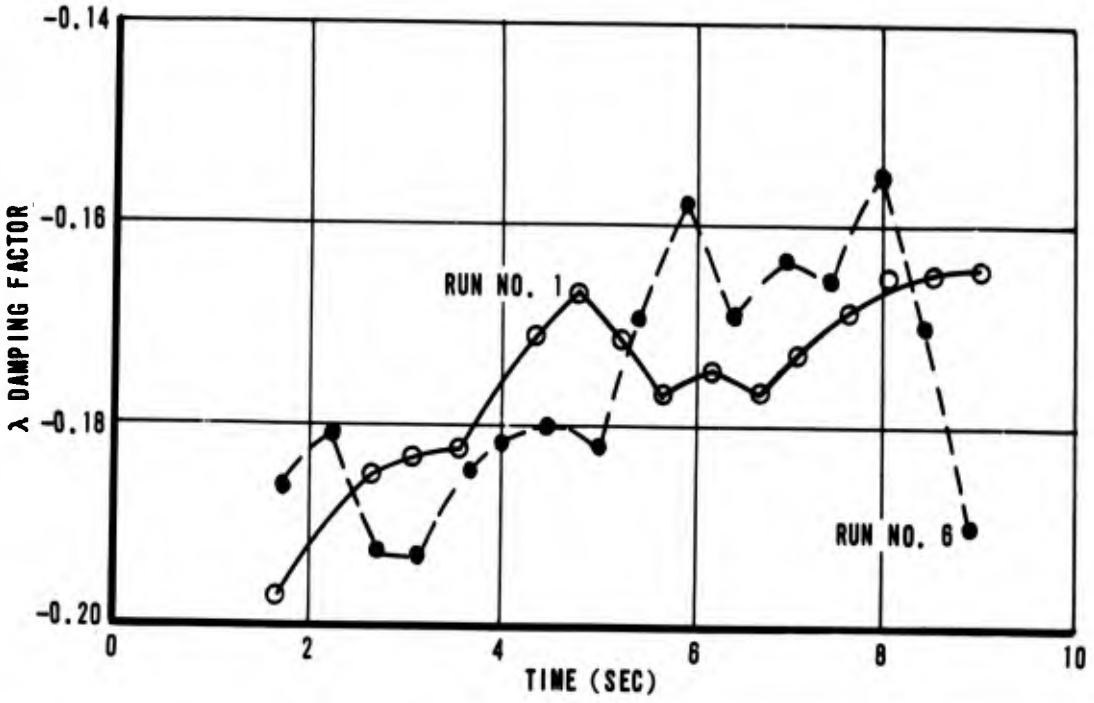

Figure 18. Variation of Damping Factor With Time.

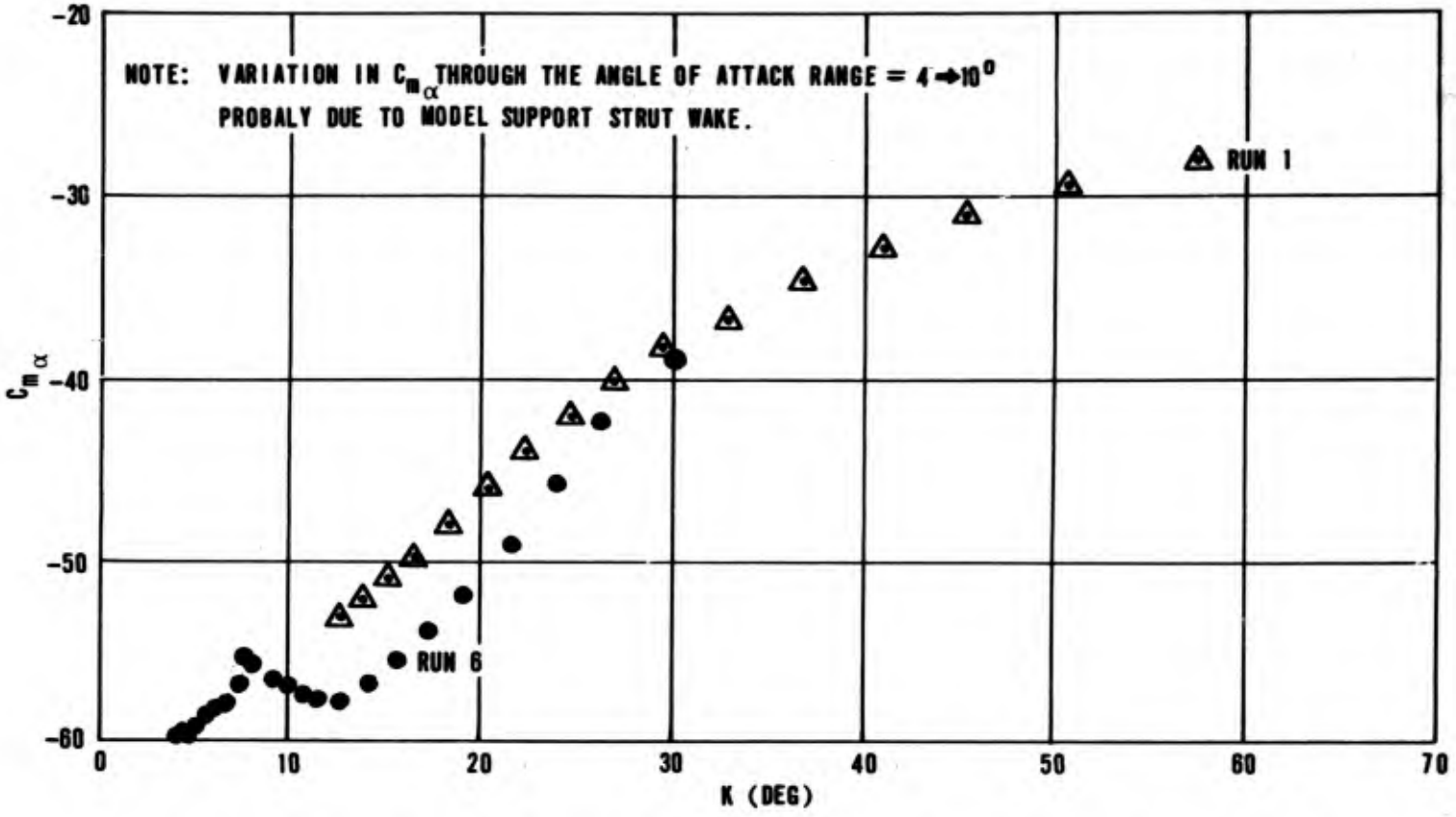

Figure 19. Variation of a Pitching Moment Curve Slope With K Amplitude.

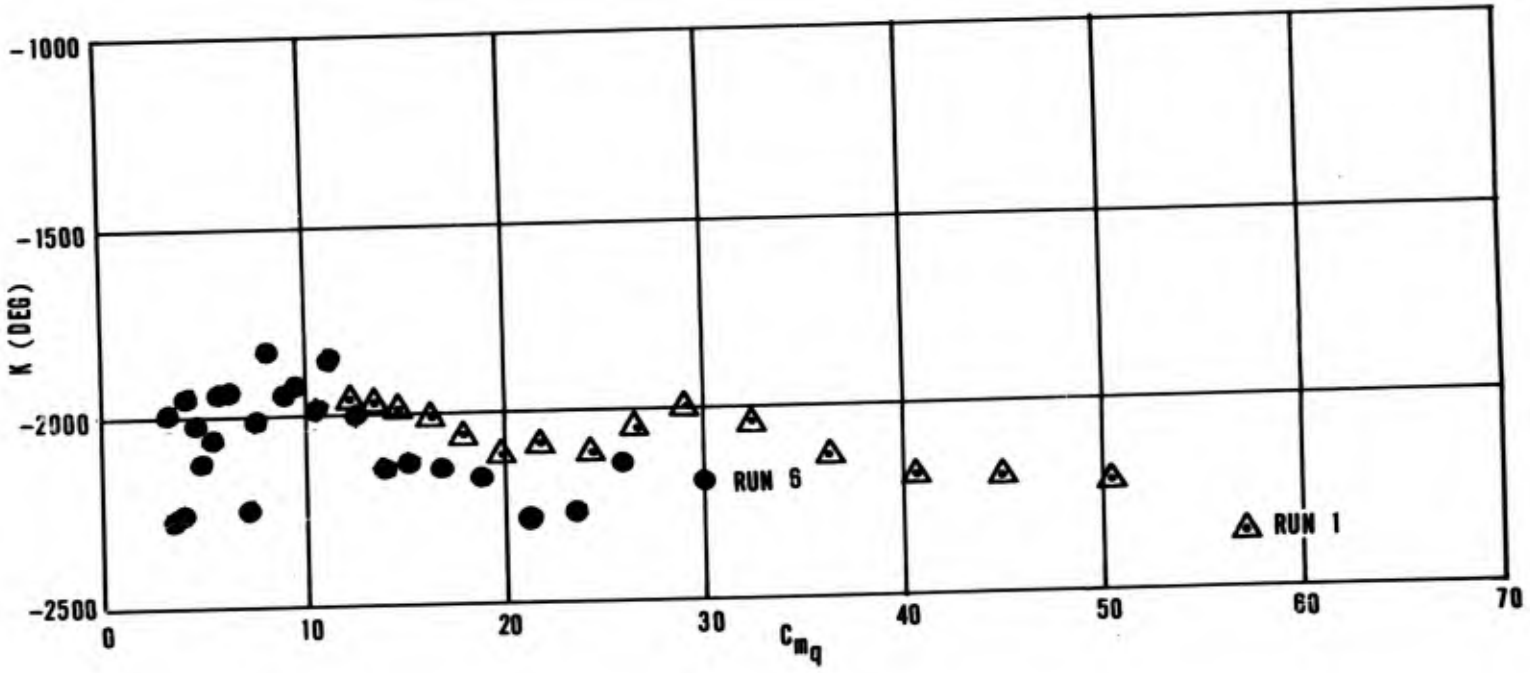

Figure 20. Variation of Pitch Damping Moment Coefficient With K Amplitude.

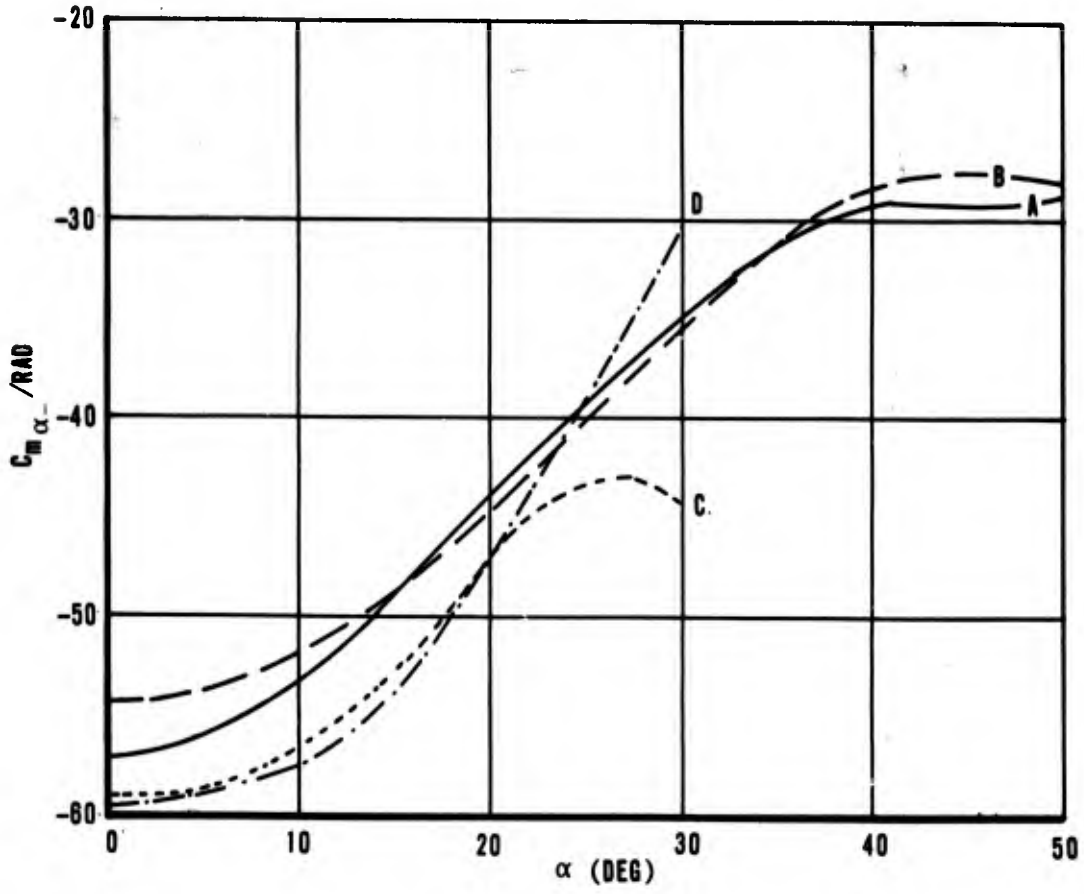

A - RUN NO. 1 $C_{m_\alpha} = -57.33 + 0.04282\,\alpha^2 - 2.2256 \times 10^{-5}\alpha^4 + 3.9791 \times 10^{-9}\alpha^6$

B - RUN NO. 1 $C_{m_\alpha} = -54.423 + 0.026744\,\alpha^2 - 0.65202 \times 10^{-5}\alpha^4$

C - RUN NO. 6 $C_{m_\alpha} = -59.277 + 0.018866\,\alpha^2 + 4.6331 \times 10^{-5}\alpha^4 - 41.027 \times 10^{-9}\alpha^6$

D - RUN NO. 6 $C_{m_\alpha} = -59.578 + 0.028544\,\alpha^2 + 0.45324 \times 10^{-5}\alpha^4$

Figure 21. Computed Variation of C_{m_α} With Angle of Attack.

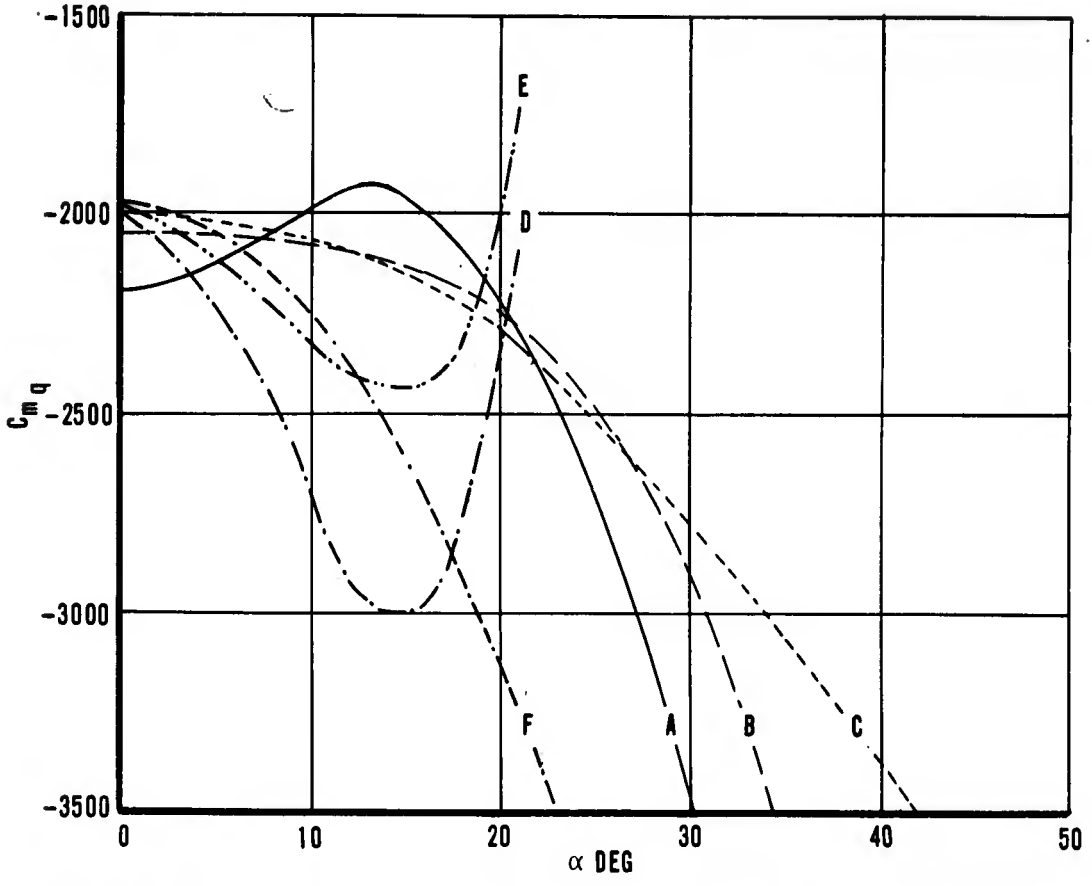

A	RUN NO. 1 $C_{m_q} = -2185.1 + 3.0212\alpha^2 \quad -1019.2\alpha^4 \times 10^{-5} + 5.9294\alpha^6 \times 10^{-6}$
B	RUN NO. 1 $C_{m_q} = -2047.0 - .1752\alpha^2 \quad -.0008313\alpha^4 \times 10^{-5}$
C	RUN NO. 1 $C_{m_q} = -1999.3 - .8511\alpha^2$
D	RUN NO. 6 $C_{m_q} = -2010.2 + 3.6518\alpha^2 \quad -10357\alpha^4 \times 10^{-5} \quad +300.46\alpha^6 \times 10^{-6}$
E	RUN NO. 6 $C_{m_q} = -1952.5 \quad -5.1089\alpha^2 \quad +1236.6\alpha^4 \times 10^{-5}$
F	RUN NO. 6 $C_{m_q} = -1978.1 \quad -2.8026\alpha^2$

Figure 22. Computed Variation of C_{m_q} With Angle of Attack.

The computed polynomials shown in Table VI expressing the coefficients as functions of angles of attack were determined from the methods of Redd and Rasmussen. The expressions shown for runs number 1 and 6 are plotted in Figures 21 and 22. The fourth and sixth degree terms are questionable in some cases, particularly in the pitch damping coefficient polynomial. Until such time that this can be resolved, it is recommended that C_{m_q} be represented by a second degree polynomial only. The expression for C_{m_α} using a fourth or sixth degree polynomial are valid through the range at angles of attack actually recorded, but not beyond. If C_{m_α} is computed for α=50° using run number 6 where $C_{m_\alpha} = -59.578 + .028544\ \alpha^2 + .45324 \times 10^{-5}\ \alpha^4$ and the maximum recorded amplitude was $\alpha \approx -24$, a value for C_{m_α} of +40.1 would result which is certainly not realistic. It is recommended that the C_{m_α} and C_{m_q} polynomial expressions determined from run No. 1 be used in further stability studies.

Care must be taken in analyzing test results with the type of sting support system used for those tests due to the flow interference effects on the fins.

Although the available data from this test were not entirely conclusive in regard to sting effects, the writer strongly suspects that the variations in C_{m_α} shown in Figure 19 from α=4 → 10 degrees are due to the strut wake and fin interaction. It is this region of angle of attack that the wake from the support system impinges on the fins resulting in a decrease in lift on the fins. An extension to the support system was added to the upper surface of the model and slightly greater decreases in lift were observed for this case, since flow interference effect would then occur on two fins. The sting effects normally must be considered carefully, since in general the angle of attack range normally of interest would be up to 15 degrees.

The sting effect would also be reflected in the computed value of C_{m_α} at zero degrees angle of attack since the fitting process using the higher ordered polynomials would result in smaller values of C_{m_α} at α=0 degrees, as compared to a smooth extrapolation of the data above ten degrees to α=0 degrees.

The recorded angle of attack time history for runs number 1 and 6 is shown in Figures 12 and 13. In order to show how well the computed sicth degree polynomials for C_{m_α} and C_{m_q} would reproduce the motion, an initial angle of attack was assumed equivalent to the first peak after zero time. With the given tunnel test condition the motion was then generated. Results of the integrations are also shown in Figures 12 and 13, and it is evident that agreement was very good.

To avoid plotting duplications, only two representative data plots of the "Wobble" program output are shown in Figures 12-18. An additional six runs with both large and small initial angles of attack were also recorded for an indication of data repeatability. These additional runs are shown in Figures 19 and 20 in the form of C_{m_α} and C_{m_q} versus K. It may be concluded that the data could be reproduced to reasonable accuracy particularly when one considers inevitable variations in tunnel conditions for successive runs.

Although scatter is apparent in the pitch damping coefficients, hopefully much of this scatter may soon be minimized by current efforts by Eikenberry in applying filtering techniques to reduce the effects of odd harmonic frequencies, and in particular the third harmonic.

Variations in pitching frequency with K amplitude is evident from Figure 16. The decreasing frequency with increasing amplitude is typical of a soft spring-type system. It has been shown in Ref. 1, that this frequency variation must be considered in the analysis of free oscillation-type data. The standard equation which has been used for years and referred to as the log decrement method is incorrect unless corrected to account for the frequency variation.

No direct comparisons of the Notre Dame test with results from the AEDC tests were possible since it was required that the current test be conducted at very low subsonic Mach numbers. The writer has conducted tests at AEDC on a sting mounted model at Mach numbers from .6 → 5.0 (Ref. 9, and 10).

One could expect that C_{m_α} as a function of Mach number may change significantly in the subsonic Mach number range from $0 < M < .6$, and thus comparing C_{m_α} for the current test to that obtained at AEDC at $M_\infty = .6$ indicates the coefficients obtained during the current test are

approximately one half the magnitude obtained by the writer at the AEDC test facility. It must also be noted that the test Reynolds number for the current test and the AEDC test were grossly different which could also account in part for these variations.

As a result of the AEDC tests and the current tests, the static and dynamic stability of the 2.75-inch FFAR at small and large angles of attack appears to be more than ample. In fact, for the particular side-firing application under study, it would be desirable that C_{m_α} be reduced to alleviate the rapid tendency for the rocket to turn toward the velocity vector. This could be accomplished by reducing the fin planform area. This would also result in improved rocket performance due to the decreased fin wave drag.

Two separate static stability tests were conducted at AEDC in the one-foot transonic model tunnel and the 40-inch supersonic test facility covering the Mach number regimes of M = .6 → 1.5 and 1.5 → 5.0, respectively. Data were obtained over an angles of attack range of -4 to 12 degrees. The test item installation for the one-foot transonic model tunnel is shown in Figure 7. This model was of identical scale (.31) with that used in the Notre Dame dynamic stability tests. The writer initiated these tests during November and December 1965 and some of these test results are published in Ref. 9 and 10. Model configuration details are shown in Figure 6.

Standard AEDC strain gage balances were supplied and calibrated by ARO personnel. The balance used in the transonic tunnel was an internal three-component balance and six-component balance was used in the supersonic tests.

From model details shown in Figure 6 it should be noted that the model used in the one-foot transonic wind tunnel required fin support tabs at the base of the fin. These tabs were necessary due to the sting type support system used and the thin cylinder wall case. These tabs of course would result in added drag and lift. To correct for the tab effect, tests were conducted with the body alone without tabs and with body alone plus tabs. The data given in Ref. 10 has not been corrected for this effect, but has been accounted for in the data given in this report.

These tests were conducted with body alone configurations and with body plus fins in order to determine fin effectiveness on static stability and also the aerodynamic characteristics of the body alone. Such that modified fin configurations could be considered at a later date.

The measured aerodynamic coefficients at $\alpha = 0$ are shown in Figure 23 for the body alone and body plus fins. The center of pressure for the body alone was found to be near the forebody ogive-cylinder juncture as is normally the case and does not vary significantly throughout the Mach number ranbe of $M\infty = .6 \rightarrow 5.0$. The addition of the fins provided a large positive static margin particularly in the transonic Mach number regime.

The drag coefficient for the body alone was as anticipated quite large. This is due to the blunt nose fuse assembly.

The static pitching moment coefficients shown in Figure 23 are referenced about the base. It is to be noted that the sign of C_{m_α} for the body alone case is (+) and (-) for the body plus fins.

Although dynamic stability tests were not conducted in either tunnel, an estimation of C_{m_q} was determined using the following equation.

$$C_{m_q} = 2\, C_{n_{\alpha_B}} \left| \frac{(X_{CP_B} - X_{CG})}{d} \right|^2 - 2\, C_{N_{\alpha_{F+I}}} \left| \frac{X_{CG} - X_{CP_{F+I}}}{d} \right|^2$$

where

$C_{N_{\alpha_B}}$ = Normal force slope for body alone.

X_{CG} = Distance from body base to center of gravity.

X_{CP_B} = Distance from body base to body alone center of pressure.

$X_{CP_{F+I}}$ = Distance from body base to fine + fin-body interference center of pressure.

$C_{N_{\alpha_{F+I}}}$ = Normal force slope for fin + body interference.

d = Model diameter.

The $C_{N_{\alpha_{F+I}}}$ used above was determined by subtracting $C_{N_{\alpha_B}}$ for the body

alone case from C_{N_α} for the body plus fins. The results of these calculations are shown in Figure 23(e). These computed values normally agree reasonably well with actual $C_{m_q} + C_{m_{\dot{\alpha}}}$ values as determined from forced or free oscillation testing since the value C_{m_α} is generally small as compared to C_{m_q}. Variations in C_N, C_m and C_A with angles of attack up to 12 degrees and for a Mach number regime of $M_\infty = .6 \rightarrow 5.0$ is shown in Table VIII.

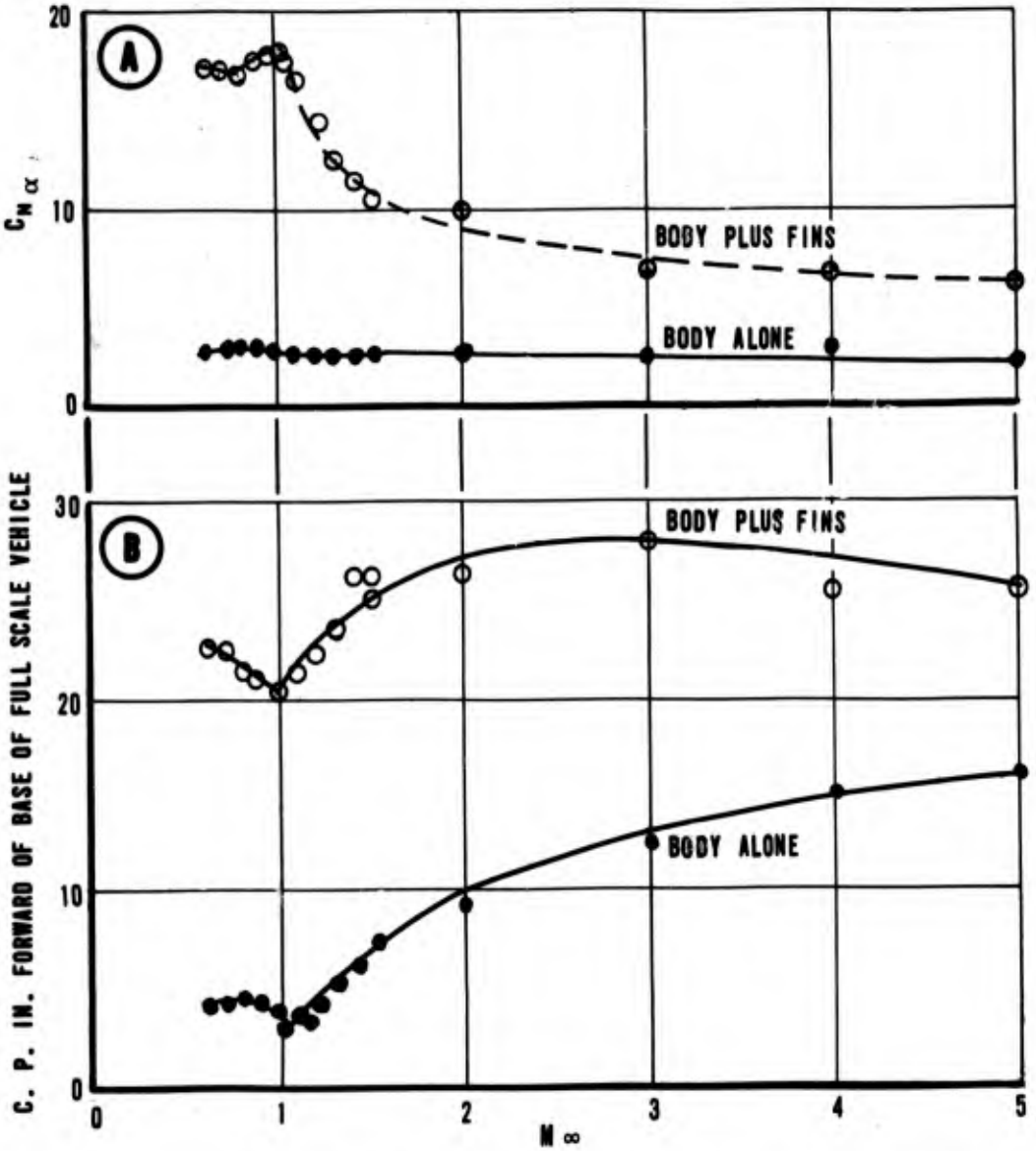

Figure 23. AEDC TEST RESULTS. (a) Variation of Normal Force Coefficient at $C_N = 0$, and (b) Variation of Center of Pressure at $C_N = 0$ With Mach Number.

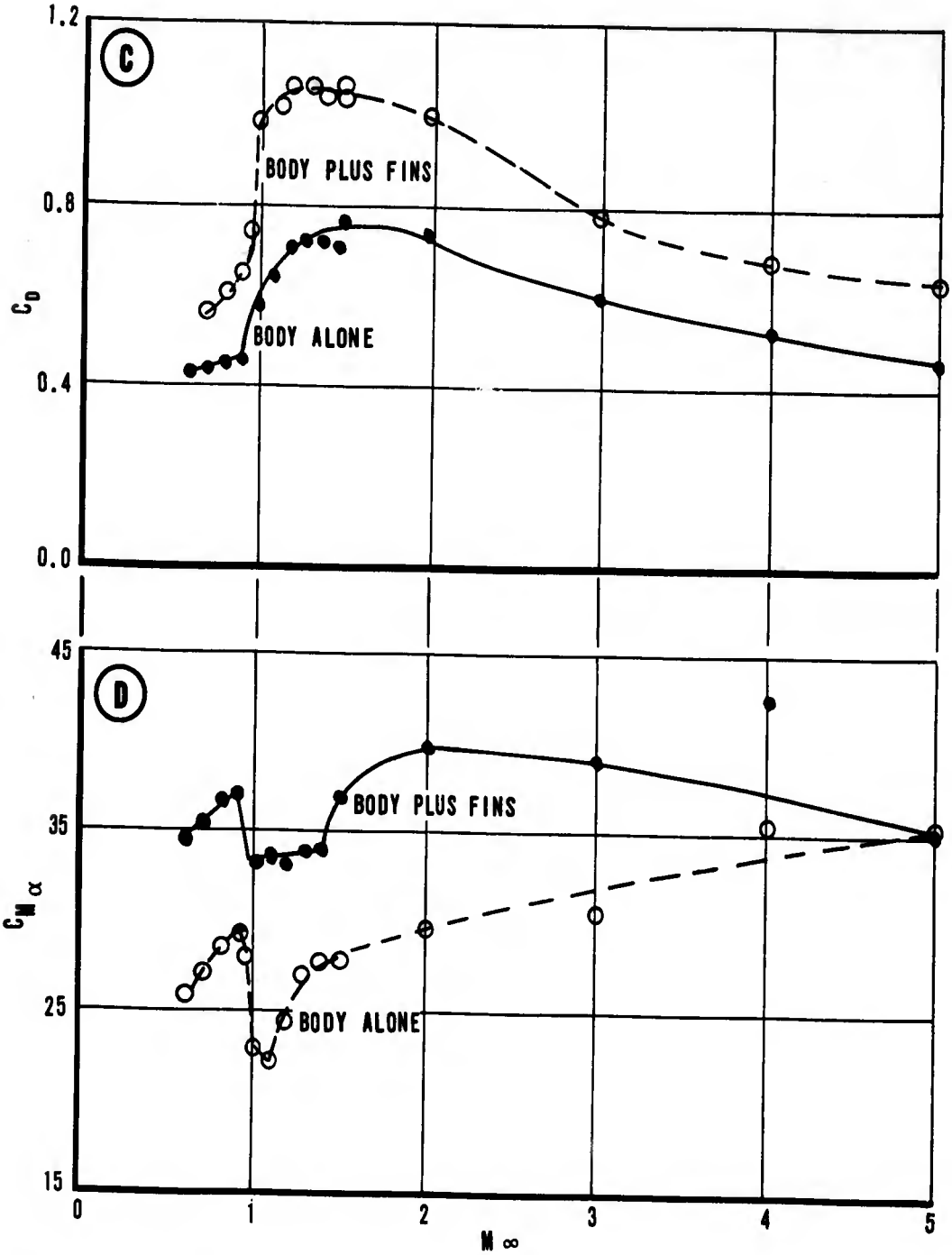

Figure 23 (c). Variation of Drag Coefficient at $C_N = 0$ With Mach Number, and (d) Variation of Static Pitching Moment Curve Slope at $C_N = 0$ With Mach Number.

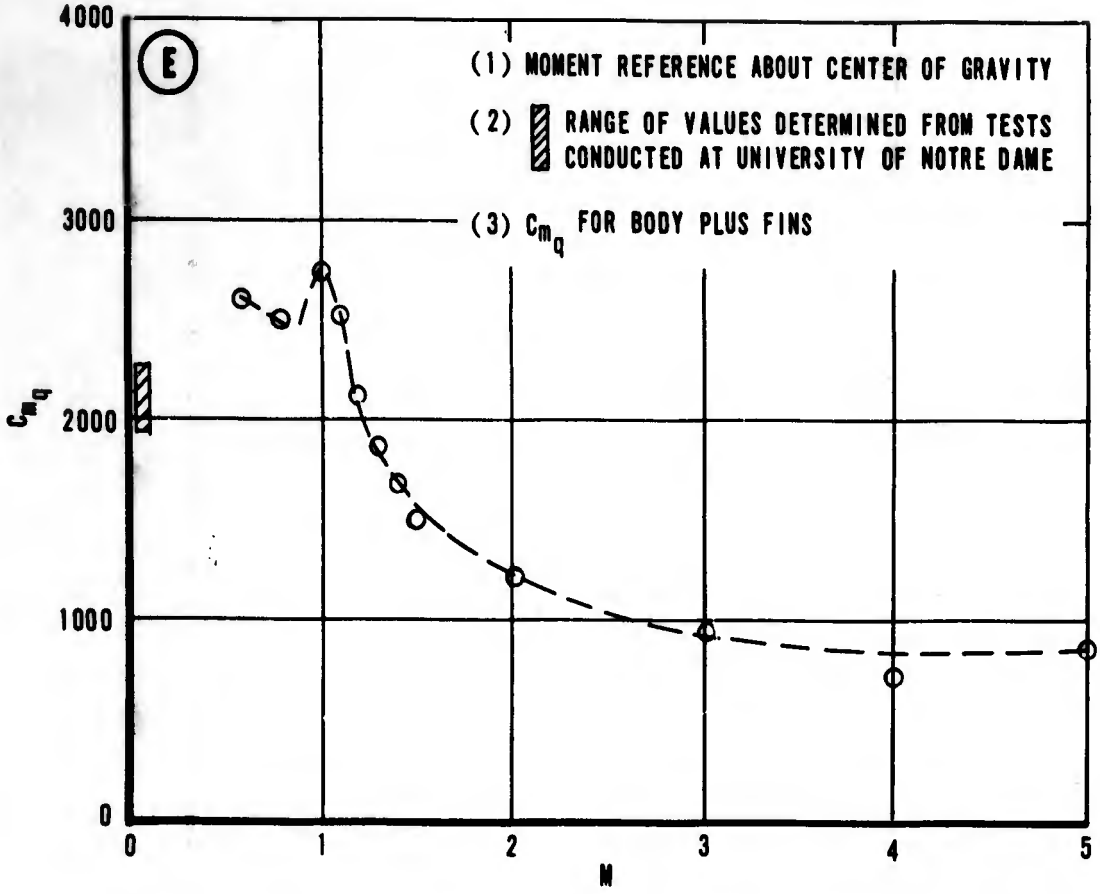

Figure 23 (e). Calculated Variation of Pitch Damping Moment Coefficient at $C_N = 0$ With Mach Number.

TABLE I. TEST CONDITIONS.

Item	Run	No.
Velocity (ft/sec)	37.96	37.49
Dynamic Pressure (lb/ft^2)	1.636	1.636
Temperature (^oF)	65	60
Density ($slugs/ft^2$)	.002271	.002328
Reynold No.	3.148×10^6	3.211×10^6

TABLE II. FIRST APPROXIMATIONS (From APRXC Subroutine).

Item	Run	No.
Trim angle of attack (α_t) (deg)	-.7582	.1906
Amplitude of (K) (deg)	51.7458	27.58
Damping factor (λ) (Non)	-.1944	-.1905
Frequency (ω) (rad/sec)	2.7720	3.2499
Phase angle (δ) (rad)	3.5112	3.6832

TABLE III(a). RESULTS FROM VARYING FREQUENCY FITTING PROCESS AND PROBABLE ERRORS (RUN NO. 1).

	T1	TM	σ_T	K	λ	ω	PE of Fit	K(PE)x100 / K	ω(PE)x100 / ω
	.00	1.65	.0735	57.2276	-.1975	2.2367			
PE			.06555	.25605	.00273	.00200	.34771	.4474	.0894
	.50	2.60	.1352	50.5024	-.1856	2.2884			
PE			.05239	.17488	.00183	.00182	.31308	.2869	.0795
	1.00	3.05	.0699	45.1205	-.1835	2.3575			
PE			.04059	.12132	.00145	.00172	.23971	.2689	.0730
	1.50	3.45	.1049	40.7019	-.1835	2.4219			
PE			.04415	.16818	.00221	.00173	.25612	.4131	.0714
	2.00	3.90	.1617	36.4508	-.1780	2.4914			
PE			.04104	.11926	.00191	.00221	.23543	.3272	.0887
	2.50	4.35	.2691	32.5786	-.1712	2.5614			
PE			.03387	.11430	.00190	.00192	.19220	.3508	.0750
	3.00	4.80	.3499	29.1810	-.1672	2.6182			
PE			.02813	.09497	.00191	.00165	.15805	.3255	.0630
	3.50	5.25	.4119	26.5609	-.1713	2.6779			
PE			.02097	.06069	.00131	.00165	.11659	.2277	.0616
	4.00	5.75	.4478	24.4114	-.1769	2.7448			
PE			.01557	.05590	.00134	.00104	.08515	.2289	.0379
	4.50	6.20	.4568	21.9949	-.1747	2.8129			
PE			.01101	.02997	.00084	.00107	.06037	.1363	.0380
	5.00	6.65	.4551	20.0021	-.1768	2.8749			
PE			.01045	.03758	.00110	.00093	.05673	.1879	.0323
	5.50	7.10	.4408	18.0759	-.1728	2.9335			
PE			.01355	.03779	.00141	.00154	.07287	.2091	.0525
	6.00	7.60	.4198	16.3736	-.1686	2.9854			
PE			.01337	.04588	.00163	.00155	.07186	.2802	.0519
	6.50	8.05	.3947	14.8505	-.1656	3.0208			
PE			.00979	.02801	.00130	.00128	.05219	.7886	.04237
	7.00	8.55	.3955	13.5680	-.1648	3.0561			
PE			.00972	.03204	.00137	.00142	.05185	.2361	.0465
	7.50	9.00	.3851	12.4428	-.1638	3.0848			
PE			.01104	.03188	.00177	.00171	.05830	.2562	.0554

TABLE III (b). RESULTS FROM VARYING FREQUENCY FITTING PROCESS AND PROBABLE ERRORS (RUN NO. 6).

	T1	TM	α_T	K	λ	ω	PE of Fit	K(PE)x100 / K	ω(PE)x100 / ω
	.00	1.65	-.7991	30.0291	-.1863	2.6576			
PE			.05031	.18395	.00356	.00352	.27184	.6126	.1258
	.50	2.25	-.6000	26.1434	-.1814	2.7503			
PE			.03168	.09522	.00222	00246	.17367	.3642	.0894
	1.00	2.70	-.5130	23.8485	-.1928	2.8582			
PE			.01804	.06082	.00152	.00150	.09805	.2550	.0525
	1.50	3.10	-.4776	21.3961	-.1931	2.9569			
PE			.02084	.06771	.00212	.00189	.11140	.3164	.0639
	2.00	3.55	-.4192	18.9668	-.1841	3.0439			
PE			.01021	.03132	.00101	.00119	.05403	.1651	.0391
	2.50	4.00	-.4158	17.0779	-.1822	3.1005			
PE			.00963	.03153	.00126	.00107	.05046	.1846	.0345
	3.00	4.50	-.4237	15.4279	-.1802	3.1469			
PE			.00799	.02388	.00097	.00115	.04186	.1548	.0365
	3.50	4.95	-.4129	14.0590	-.1820	3.1797			
PE			.00859	.02777	.00136	.00120	.04451	.1975	.0377
	4.00	5.45	-.3710	12.6550	-.1692	3.2098			
PE			.01190	.03527	.00180	.00205	.06168	.2787	.06387
	4.50	5.95	-.3202	11.4188	-.1572	3.2077			
PE			.01255	.03918	.00234	.00208	.06513	.3433	.0648
	5.00	6.45	-.2725	10.6441	-.1683	3.1985			
PE			.00672	.02045	.00122	.00135	.03489	.1921	.0422
	5.50	6.95	-.3089	9.7238	-.1635	3.1858			
PE			.01316	.04020	.00286	.00262	.06839	.4134	.0822
	6.00	7.45	-.3219	9.0128	-.1655	3.1766			
PE			.01184	.03672	.00257	.00277	.06159	.4074	.0872
	6.50	7.95	-.2825	8.1938	-.1553	3.1568			
PE			.01160	.03456	.00292	.00275	.06037	.4218	.0871

TABLE III (b). CONCLUDED.

	T1	TM	α_T	K	λ	ω	PE of Fit	K(PE)x100 / K	ω(PE)x100 / ω
PE	7.00	8.45	-.2442 .01019	7.6821 .03229	-.1710 .00265	3.1425 .00279	.05303	.4203	.0888
PE	7.50	8.95	-.1706 .01550	7.2369 .04759	-.1904 .00471	3.1841 .00436	.08048	.6576	.1369
PE	8.00	9.45	-.1159 .00313	6.3917 .00969	-.1643 .00095	3.2179 .00105	.01621	.1516	.0326
PE	8.50	9.95	-.1192 .00351	5.8833 .01059	-.1646 .00128	3.2241 .00116	.01818	.1800	.03597
PE	9.00	10.45	-.1077 .00489	5.4581 .01559	-.1748 .00179	3.2309 .00194	.02533	.2856	.0600
PE	9.50	10.95	-.0927 .00497	5.0429 .01488	-.1805 .00215	3.2516 .00200	.02567	.2951	.0615
PE	10.00	11.40	-.0803 .00436	4.5581 .01404	-.1710 .00197	3.2699 .00208	.02225	.3080	.0636
PE	10.50	11.90	-.0604 .00530	4.1377 .01515	-.1655 .00274	3.2626 .00266	.02707	.3661	.0815
PE	11.00	12.40	-.0361 .00423	3.8927 .01426	- 1904 .00236	3.2655 .00238	.02155	.3663	.0728
PE	11.50	12.90	-.0224 .00388	3.5545 .01093	-.1925 .00238	3.3012 .00240	.01974	.3074	.0727
PE	12.00	13.40	-.0059 .00517	3.1453 .01744	-.1694 .00354	3.3193 .00342	.02630	.5545	.1030

TABLE IV. ACCURACY OF VARIABLE FREQUENCY FITTING PROCESS AS APPLIED TO AMPLUTUDE (K) AND FREQUENCY (ω).

Run No.	K Average for All Section Fits	ω Average for All Section Fits
1	.2732	.0599
6	.3280	.0686

TABLE V (a). C_{m_α} AND C_{m_q} FOR VARIOUS SECTION FITS (RUN NO. 1).

TI	TM	C_{m_α}	C_{m_α} PE	C_{m_q}	C_{m_q} PE
.00	1.65	-28.02	.04	-2352.91	23.01
.50	2.60	-29.33	.03	-2211.50	15.45
1.00	3.05	-31.13	.03	-2186.37	12.24
1.50	3.45	-32.86	.03	-2185.62	18.60
2.00	3.90	-34.77	.04	-2120.06	16.08
2.50	4.35	-36.75	.04	-2039.05	16.01
3.00	4.80	-38.40	.03	-1991.73	16.07
3.50	5.25	-40.17	.03	-2040.23	11.03
4.00	5.75	-42.20	.02	-2107.24	11.27
4.50	6.20	-44.32	.02	-2081.43	7.12
5.00	6.65	-46.29	.02	-2105.80	9.30
5.50	7.10	-48.20	.04	-2058.54	11.91
6.00	7.60	-49.92	.04	-2008.63	13.75
6.50	8.05	-51.11	.03	-1972.91	10.95
7.00	8.55	-52.31	.03	-1963.36	11.52
7.50	9.00	-53.30	.04	-1951.79	14.92

TABLE V (b). C_{m_α} AND C_{m_q} FOR VARIOUS SECTION FITS (RUN NO. 6).

TI	TM	C_{m_α}	C_{m_α} PE	C_{m_q}	C_{m_q} PE
.00	1.65	-38.97	.07	-2192.00	29.62
.50	2.25	-42.37	.05	-2134.58	18.49
1.00	2.70	-45.76	.03	-2268.36	12.64
1.50	3.10	-48.98	.04	-2272.12	17.61
2.00	3.55	-51.90	.03	-2165.29	8.41
2.50	4.00	-53.85	.03	-2142.94	10.46
3.00	4.50	-55.47	.03	-2120.02	8.10
3.50	4.95	-56.63	.03	-2141.39	11.31
4.00	5.45	-57.71	.05	-1990.05	14.96
4.50	5.95	-57.63	.05	-1849.90	19.46
5.00	6.45	-57.30	.03	-1979.44	10.17
5.50	6.95	-56.85	.07	-1924.01	23.78
6.00	7.45	-56.52	.07	-1946.76	21.38
6.50	7.95	-55.82	.07	-1826.95	24.26
7.00	8.45	-55.31	.07	-2011.44	22.08
7.50	8.95	-56.79	.11	-2240.53	39.19
8.00	9.45	-58.00	.03	-1933.43	7.89
8.50	9.95	-58.23	.03	-1935.84	10.62
9.00	10.45	-58.47	.05	-2056.02	14.89
9.50	10.95	-59.22	.05	-2123.76	17.88
10.00	11.40	-59.89	.05	-2011.80	16.43
10.50	11.90	-59.62	.07	-1947.40	22.77
11.00	12.40	-59.73	.06	-2240.40	19.66
11.50	12.90	-61.04	.06	-2265.03	19.79
12.00	13.40	-61.71	.09	-1993.14	29.47

TABLE VI (a). COMPUTED SECOND, FOURTH, AND SIXTH DEGREE POLYNOMIALS FOR C_{m_q}.

$C_{m_q} = C_0 + C_2\alpha^2$

Run	C_0	C_2
1	-1999.3	-.8511
6	-1978.1	-2.8026

$C_{m_q} = C_0 + C_2\alpha^2 + C_4\alpha^4$

Run	C_0	C_2	$C_4 \times 10^{-5}$
1	-2047.0	-.1752	-83.13
6	-1952.5	-5.1089	1236.6

$C_{m_q} = C_0 + C_2\alpha^2 + C_4\alpha^4 + C_6\alpha^6$

Run	C_0	C_2	$C_4 \times 10^{-5}$	$C_6 \times 10^{-6}$
1	-2185.1	3.0212	-1019.2	5.9294
6	-2010.2	3.6518	-10357.0	300.46

TABLE VI (b). COMPUTED SECOND, FOURTH, AND SIXTH DEGREE POLYNOMIALS FOR C_{m_α}.

$C_m = C_0 + C_2\alpha^2$

Run	C_0	C_2
1	-49.601	.011137
6	-59.721	.031232

$C_m = C_0 + C_2\alpha^2 + C_4\alpha^4$

Run	C_0	C_2	$C_4 \times 10^{-5}$
1	-54.423	.026744	-.65202
6	-59.578	.028544	.45324

$C_{m_\alpha} = C_0 + C_2\alpha^2 + C_4\alpha^4 + C_6\alpha^6$

Run	C_0	C_2	$C_4 \times 10^{-5}$	$C_6 \times 10^{-9}$
1	-57.330	.042082	-2.2256	3.9791
6	-59.277	.018866	4.6331	-41.027

TABLE VII. VARIATIONS IN PROBABLE ERRORS IN C_{m_α} AND C_{m_q} RESIDUALS FOR SECOND, FOURTH, AND SIXTH DEGREE POLYNOMIALS REPRESENTING THE COEFFICIENTS AS A FUNCTION OF K AMPLITUDE.

OVERALL PROBABLE ERROR IN C_{m_α} RESIDUALS FOR VARIOUS POLYNOMIALS REPRESENTING (C_{m_α} vs K)			
Run	2nd	4th	6th
1	2.377	.982	.4018
6	.9000	.9137	.915

OVERALL PROBABLE ERROR IN C_{m_q} RESIDUALS FOR VARIOUS ORDERED POLYNOMIALS REPRESENTING (C_{m_q} vs K)			
Run	2nd	4th	6th
1	33.78	32.8	29.13
6	72.57	72.94	70.39

TABLE VIII. VARIATION OF C_N, C_m AND C_A WITH MACH NUMBER AND ANGLE OF ATTACK AS DETERMINED FROM AEDC STATIC STABILITY TEST.

M = 0.6

$\frac{R}{ft} = 3.83 \times 10^{+6}$

α	C_N	C_m	C_A
-4.05	-.957	-1.678	.494
-2.02	-.601	- .723	.505
0.0	-.041	.036	.495
2.02	.619	.708	.497
4.05	.982	1.689	.493
6.09	1.351	2.781	.595
8.14	1.750	4.057	.497
10.19	2.197	5.523	.534
12.26	2.526	7.234	.570

M = 0.8

$\frac{R}{ft} = 4.50 \times 15^{+6}$

α	C_N	C_m	C_A
-4.07	-1.018	-1.595	.530
-2.02	.593	- .656	.526
.01	- .008	.081	.520
2.03	.610	.798	.5211
4.08	1.071	1.735	.527
6.18	1.488	2.829	.530
8.21	1.889	4.185	.558
10.31	2.211	5.857	.606
12.42	2.566	7.760	.647

M = 1.0

$\frac{R}{ft} = 4.81 \times 10^{+6}$

α	C_N	C_m	C_A
-4.07	-1.149	-1.502	.977
-2.02	.627	- .629	.951
.0	.009	.065	.941
2.04	.640	.777	.952
4.09	1.165	.167	.971
6.16	1.635	2.770	.979
8.27	1 999	4.273	.977
10.39	2.425	6.049	.981
12.54	2.829	7.999	.980

M = 1.2

$\frac{R}{ft} = \frac{4}{97} \times 10^{+6}$

α	C_N	C_m	C_A
-4.10	-.977	-1.655	.998
-2.04	-.533	- .668	.973
.01	-.008	.158	.959
2.07	.527	1.002	.977
4.14	1.000	2.026	.997
6.23	1.467	3.234	1.003
8.34	1.946	4.721	1.014
10.50	2.381	6.691	1.022
12.70	2.775	9.006	1.011

TABLE VIII. CONCLUDED.

M = 2

$\frac{R}{ft} = .41 \times 10^{+6}$

α	C_N	C_m	C_A
-3.91	-.60	-2.38	1.017
- .83	-.257	- .909	.987
- .0158	-.009	- .106	.983
2.13	.316	1.09	.988
4.10	.597	2.26	1.017
6.13	.945	3.99	1.039
8.13	1.32	6.10	1.054
10.15	1.74	8.90	1.050
12.23	2.27	12.9	1.044

M = 3

$\frac{R}{ft} = .62 \times 10^{+6}$

α	C_N	C_m	C_A
-3.95	-.558	-2.811	.809
-1.85	-.238	-1.175	.775
+ .0861	-.686	- .081	.768
2.15	.262	1.198	.779
4.14	.5389	2.606	.808
6.18	.865	4.456	.820
8.23	1.287	12.52	.833
10.35	1.836	11.28	.832
12.48	2.540	16.29	.832

M = 4

$\frac{R}{ft} = .51 \times 10^{+6}$

α	C_N	C_m	C_A
-3.92	-.463	-2.639	.676
-1.83	-.207	-1.056	.670
- .003	-.007	- .087	.670
2.14	.232	1.243	.671
4.10	.450	2.471	.674
6.13	.819	4.612	.689
8.15	1.30	7.775	.700
10.16	1.809	11.24	.711
12.20	2.400	15.30	.721

M = 5

$\frac{R}{ft} = .53 \times 10^{+6}$

α	C_N	C_m	C_A
-4.06	- .469	-2.739	.630
-1.97	- .172	.977	.614
- .05	- .024	- .124	.620
1.94	+ .187	.127	.61
3.89	.434	2.547	.625
5.99	.796	4.772	.646
7.99	1.229	7.618	.659
9.99	1.690	10.665	.676
12.01	2.232	14.234	.683

Note: Above data were not corrected for fin tab effect.

CONCLUSIONS

1. The following polynomial expressions are recommended for further stability studies $C_{m_\alpha} = 57.33 + .042082\,\alpha^2 - 2.2256 \times 10^{-5}\,\alpha^4 + 3.9791\alpha^6 \times 10^{-9}$ $C_{m_q} = -1999.3 - .8511\,\alpha^2$.

2. The percentage errors in amplitude (K) and frequency (ω) as determined from the variable frequency fitting subroutine were .4417 and .0944 percent, respectively.

3. The static and dynamic stability characteristics of the 2.75-inch FFAR is satisfactory at both small and large angles of attack.

4. It is recommended that the fin plan form area be reduced to decrease C_{m_α} and the associated turning of the rocket into the relative velocity vector. Although secondary, the rocket performance would be improved due to the reduced fin wave drag.

5. "Wobble" provides an excellent tool for determining C_{m_α} and C_{m_q} at large angles of attack, and should be incorporated in future free oscillation testing in wind tunnels with greater Mach number capability.

6. Use of jewel bearings in the free oscillation model support system results in minimal bearing friction.

7. Wake effects using the transverse rod-type support systems should be investigated using various diameter support rods and fin orientations. This investigation should be of a nature such that wake effects on the body and fins may be minimized, or at least corrected for.

8. Use of the low turbulance Notre Dame test facilities provides the flexibility for an excellent tool for dynamic stability studies at large angles of attack.

9. Improvements in rocket performance by reduced drag would be realized with slight modification of the external portion of the warhead fuze.

10. Additional tests should be conducted in the Mach number regime of .2 → 1.3 using single and multidegree of freedom support systems. The "Wobble" computer program should be utilized in the analysis. In addition, static stability characteristics should be obtained at Mach number less than $M_\infty = .6$ and variations of angles of attack up to $\alpha = 90$ degrees.

REFERENCES

1. Nicolaides, John D., Missile Flight and Astrodynamics, TN 100a, Bureau of Naval Weapons, 1961.

2. Eikenberry, R. S., "Wobble", A Computer Program for the Analysis of Quadracyclic Missile Motions, Aerospace Engineering Department, University of Notre Dame.

3. Rausmussen, Maurice L., Kirk, D. B., A Study of Damping in Nonlinear Oscillations, NASA TR R-249, October 1966.

4. Redd, Bass, Olsen, Dennis, M. Barton, Richard L., Relationship Between the Aerodynamic Damping Derivatives Measured as a Function of Instantaneous Angular Displacement and the Aerodynamic Damping Derivatives Measured as a Function of Oscillation Amplitude, NASA, June 1965.

5. Nelson, R., Oras, J., Faller, T., Flight Dynamics of Aircraft Munitions. Report of Summer 1965 under AF Contract 08 635-5275.

6. Martinelli, E., Eglin FFAR tests, Project 670A, National Data Reports Nos. NR-AN-1134, NR-AN-1179, NR-AN-1229, March 1967.

7. Bliss, Gilbert A., Mathematics for Exterior Ballistics, 1944.

8. Kryloff, N., and Bogolinboff, N., Introduction to Nonlinear Mechanics. Princeton, 1943 105 pp. Trans. from Russian Revision Published in 1937.

9. Hilliard, E.E., and Myers, A.W., Aerodynamics Characteristics of 2.75-Inch Folding Fin Aircraft Rocket at Supersonic Speeds AEDC-TR-65-267, December 1965.

10. Black, John A., Force Tests of Seven Configurations of a Folding Fin Aircraft Rocket at Transonic Speeds AEDC-TR-65-248.

11. Nicolaides, John D., Eikenberry, R.S., Ingram, C.W., The Determination of Aerodynamics Stability Coefficients From Sounding Rocket Flight Data. Aero-Space Engineering Department, University of Notre Dame.

12. Cunningham, W.J., Introduction to Non-Linear Analysis, 1958.

INITIAL DISTRIBUTION

20	DDC
1	AUL-9764
	Eglin AFB
30	ATBR
7	ADBPS-12
3	ADEH
2	ADTPR

UNCLASSIFIED
Security Classification

DOCUMENT CONTROL DATA - R & D

(Security classification of title, body of abstract and indexing annotation must be entered when the overall report is classified)

1. ORIGINATING ACTIVITY *(Corporate author)*
Air Force Armament Laboratory
Eglin Air Force Base, Florida

2a. REPORT SECURITY CLASSIFICATION
UNCLASSIFIED

2b. GROUP
---

3. REPORT TITLE
2.75-INCH FFAR LARGE YAW DYNAMICS

4. DESCRIPTIVE NOTES *(Type of report and inclusive dates)*
---

5. AUTHOR(S) *(First name, middle initial, last name)*
Carroll B. Butler

6. REPORT DATE
March 1968

7a. TOTAL NO. OF PAGES
82

7b. NO. OF REFS
12

8a. CONTRACT OR GRANT NO.
---

b. PROJECT NO.

c.

d.

9a. ORIGINATOR'S REPORT NUMBER(S)
AFATL-TR-68-43

9b. OTHER REPORT NO(S) *(Any other numbers that may be assigned this report)*

10. DISTRIBUTION STATEMENT This document is subject to special export controls and each transmittal to foreign governments or foreign nationals may be made only with prior approval of the Air Proving Ground Center, Air Force Armament Laboratory (ATBR), Eglin Air Force Base, Florida 32542.

11. SUPPLEMENTARY NOTES
Available in DDC

12. SPONSORING MILITARY ACTIVITY
Air Force Armament Laboratory
Eglin Air Force Base, Florida 32542.

13. ABSTRACT
Dynamic tests were conducted in the 24-inch Subsonic Wind Tunnel at the Notre Dame Aero-Space Department to investigate primarily the large yaw dynamic characteristics of the 2.75-inch FFAR, utilizing a unique model support system which provides single degree of freedom motion. From the free pitching motion the stability coefficients C_{m_α} and C_{m_q} were obtained for the 2.75-inch FFAR at low subsonic Mach numbers, and at angles of attack up to 60 degrees by fitting the motion to the Linear Theory utilizing the Method of Differential Corrections. Nonlinear effects due to variations in free oscillation frequency are considered. Static test results are also included from tests conducted at the Arnold Engineering Development Center. These latter tests were conducted over a Mach number regime of $M_\infty = .6 \rightarrow 5.0$ and angle of attack range of $\alpha = -4 \rightarrow 12$ degrees.

DD FORM 1 NOV 65 1473

UNCLASSIFIED
Security Classification

14. KEY WORDS	LINK A		LINK B		LINK C	
	ROLE	WT	ROLE	WT	ROLE	WT
Dynamic stability 2.75-inch FFAR Wind tunnel testing techniques						